AD-A130 346 AN EVALUATION OF VISCOELASTIC COATINGS AS LOW FREQUENCY 1/1
ACOUSTIC ABSORBERS(U) DYNAMICS TECHNOLOGY INC TORRANCE
CA Y CHEN ET AL. MAY 83 DTN-8265-01 N00014-82-C-0769

UNCLASSIFIED F/G 20/1 NL

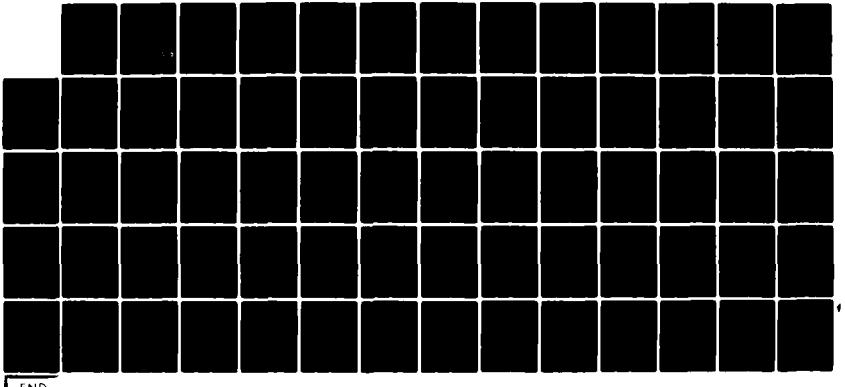

END
DATE FILMED
8 83
DTIC

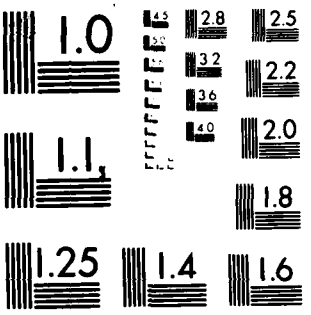

(12)

Dynamics Technology, Inc.

DTN-8256-01

AN EVALUATION OF VISCOELASTIC COATINGS AS LOW FREQUENCY ACOUSTIC ABSORBERS

May 1983

By: Y. M. Chen and R. L. Gran

Submitted to: Dr. E. Y. Harper
Office of the Chief of Naval Operations
OP-021T, 4D544
PENTAGON
Washington, D.C. 20350

Dynamics Technology, Inc.
22939 Hawthorne Blvd., Suite 200
Torrance, California 90505
(213) 373-0666

This report has undergone an extensive internal review before release, both for technical and non-technical content, by the Division Manager and an independent internal review committee.

Division Manager:

David D'Amantram

Internal Review:

C. M. Davis

UNCLASSIFIED

SECURITY CLASSIFICATION OF THIS PAGE (When Data Entered)

REPORT DOCUMENTATION PAGE		READ INSTRUCTIONS BEFORE COMPLETING FORM
1. REPORT NUMBER DTN-8265-01	2. GOVT ACCESSION NO. AD-A130 346	3. RECIPIENT'S CATALOG NUMBER
4. TITLE (and Subtitle) AN EVALUATION OF VISCOELASTIC COATINGS AS LOW FREQUENCY ACOUSTIC ABSORBERS		5. TYPE OF REPORT & PERIOD COVERED FINAL September 1982 - May 1983 6. PERFORMING ORG. REPORT NUMBER DTN-8265-01
7. AUTHOR(s) Yie-Ming Chen and Robert L. Gran		8. CONTRACT OR GRANT NUMBER(s) N00014-82-C-0769
9. PERFORMING ORGANIZATION NAME AND ADDRESS Dynamics Technology, Inc. 22939 Hawthorne Blvd., Suite 200 Torrance, CA 90505		10. PROGRAM ELEMENT, PROJECT, TASK AREA & WORK UNIT NUMBERS
11. CONTROLLING OFFICE NAME AND ADDRESS Office of Naval Research Department of the Navy 800 N. Quincy, Arlington, VA 22217	N00014	12. REPORT DATE May 1983 13. NUMBER OF PAGES 66
14. MONITORING AGENCY NAME & ADDRESS (if different from Controlling Office) Office of the Chief of Naval Operations OP-021T, 4D544 PENTAGON Washington, D.C. 20350		15. SECURITY CLASS. (of this report) UNCLASSIFIED 15a. DECLASSIFICATION DOWNGRADING SCHEDULE

16. DISTRIBUTION STATEMENT (of this Report)
Unlimited

17. DISTRIBUTION STATEMENT (of the abstract entered in Block 20, if different from Report)
Unlimited

18. SUPPLEMENTARY NOTES

19. KEY WORDS (Continue on reverse side if necessary and identify by block number)
anechoic coatings
low frequency acoustic absorbers
viscoelastic dynamic properties
target strength reduction

20. ABSTRACT (Continue on reverse side if necessary and identify by block number)
This study examines the effectiveness of elastomer coatings for specular, acoustic backscatter reduction in low frequency, under-water applications. Four representative elastomers were selected: Butyl B252, Neoprene W, Polybutadiene, and Thiokol RD. Their coating reflection loss for CW and impulse incident acoustic plane waves was examined using techniques and computer codes developed based on a geometric acoustics approach. The performance of these elastomer coatings was examined in the frequency range from 10 Hz to 10 kHz, the pressure range 0 to 500 psig, and the temperature range

DD FORM 1 JAN 73 1473 EDITION OF 1 NOV 65 IS OBSOLETE

UNCLASSIFIED

SECURITY CLASSIFICATION OF THIS PAGE (When Data Entered)

0^{o} to 30^{o}C; ranges commonly encountered in oceanic applications. The results indicate that at low frequencies (order 100 Hz), the available elastomers, applied as homogeneous coatings up to 20 cm thick, are not sufficient to obtain reflection reduction greater than 6 dB for the specified conditions. Greater specular backscatter reduction may be achieved by using layered, inhomogeneous coatings, but a more relevant approach for these low frequencies may involve the examination of structural resonant response to the incident acoustic field since the body size and acoustic wavelength are of the same order of magnitude (Gaunard, 1977). The structural resonant mechanism of backscatter is probably dominant at low frequencies.

ACKNOWLEDGEMENTS

The technical monitor for this study is Dr. E.Y. Harper of OP-021T. The authors wish to acknowledge the valuable technical discussions with T. Kubota, G. Donohue, C. M. Dube, V. Panico, D. Mantrom and D. Hove at Dynamics Technology. We would especially like to acknowledge the assistance and cooperation of Dr. W. Madigosky of NSWC for providing much of the materials data and instructive technical discussions.

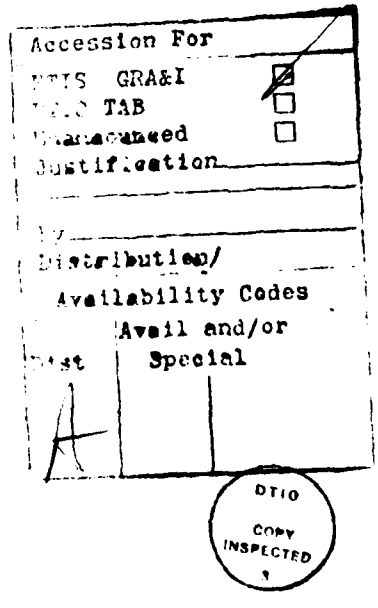

ABSTRACT

This study examines the effectiveness of elastomer coatings for specular, acoustic backscatter reduction in low frequency, underwater applications. Four representative elastomers were selected: Butyl B252, Neoprene W, Polybutadiene, and Thiokol RD. Their coating reflection loss for CW and impulse incident acoustic plane waves was examined using techniques and computer codes developed based on a geometric acoustics approach. The performance of these elastomer coatings was examined in the frequency range from 10 Hz to 10 kHz, the pressure range 0 to 500 psig, and the temperature range 0° to 30°C; ranges commonly encountered in oceanic applications. The results indicate that at low frequencies (order 100 Hz), the available elastomers, applied as homogeneous coatings up to 20 cm thick, are not sufficient to obtain reflection reduction greater than 6 dB for the specified conditions. Greater specular backscatter reduction may be achieved by using layered, inhomogeneous coatings, but a more relevant approach for these low frequencies may involve the examination of structural resonant response to the incident acoustic field since the body size and acoustic wavelength are of the same order of magnitude (Gaunard, 1977). The structural resonant mechanism of backscatter is probably dominant at low frequencies.

TABLE OF CONTENTS

LIST OF FIGURES

TABLE OF SYMBOLS

a_T	WLF frequency shift coefficient
C_a, C_b	WLF empirical shift constants
c	complex dilatational wave speed or sound speed ($c = c_r + i\ c_i$)
c_G	shear wave speed (complex)
G	complex shear modulus ($G = G_r + i\ G_i$)
H	layer thickness
I	reflected impulse response
I_s	reflected response to an arbitrary signal
K	complex bulk modulus
M	complex longitudinal modulus ($M = M_r + i\ M_i$)
P_{inc}	incident pressure amplitude
P_{refl}	reflected pressure amplitude
R	plane wave, pressure amplitude reflection coefficient
R_{12}	boundary reflection coefficient (between medium 1 and 2)
$S(\omega)$	*spectral decomposition of incident signal*
T	temperature
T_o	reference temperature
t	time variable
x,z	position variables
δ_G	loss factor or loss tangent for shear ($\delta_G = G_i/G_r$)
δ_M	longitudinal loss factor ($\delta_M = M_i/M_r$)
θ	incidence angle
λ	Lamé constant
ν	Poisson's ratio (ratio between lateral contraction and longitudinal extension)
ρ	density
ρ_1, c_1	density and sound speed in medium 1 (fluid)
ρ_2, c_2	density and sound speed in medium 2 (layer)
τ	characteristic time variable
ϕ	phase term
ω	acoustic frequency

1. INTRODUCTION

1.1 Project Objectives

There is currently some interest and concern in the U.S. Navy regarding low-frequency, active, acoustic ASW systems. If low frequency (~ 100 Hz) acoustic pulses were to be utilized, such systems might allow long-range detection (because of negligible sea-water absorption) and they might be difficult to counter with an active system onboard the target. The potential for passive countermeasures, such as anechoic coatings, has not been completely ruled out however. In particular for anechoic coatings, several recent preliminary calculations (see below) have indicated a surprising capability and it was the purpose of this investigation to refine these calculations and extend them to other possible coating materials.

The technical objective of this study is to assess the effectiveness of low frequency anechoic coatings on target strength reduction and make recommendations concerning their development and utility. In particular, acoustic reflection characteristics of a homogeneous viscoelastic layer (an elastomer coating) at low frequencies (on the order of 100 Hz) in water are examined. The effects of viscoelastic material properties and coating thickness on the reflection response are analyzed. Selected elastomers are examined for their effectiveness in this application over the range of environmental conditions to be encountered using computer codes developed to calculate the continuous, plane-wave, acoustic reflection coefficient and the impulse reflection response of a homogeneous, plane coating overlying a rigid, perfect reflecting structure.

1.2 Background and Scope

1.2.1 Background

Interest in low frequency, underwater acoustic absorbers was sparked by results of a study by G. V. Borgiotti (1981) which indicated that at 100 Hz reflection reduction on the order of 10 dB was possible with coating

thicknesses on the order of 30 cm for the elastomer Thiokol RD.* R. L. Gran (1982) corrected Borgiotti's calculations and found that reflection reduction of this level could be achieved with coating thicknesses on the order of 5 cm (Figure 1-1). After more detailed study of the typical properties of viscoelastic materials, it has been found that the encouraging conclusions of these two previous studies were the result of an underestimate for the Poisson ratio of Thiokol RD which is about 0.495 rather than 0.44 taken by the two studies. Unfortunately, the more realistic value of $\nu = 0.495$ results in much poorer reflection reduction as discussed later in this report.

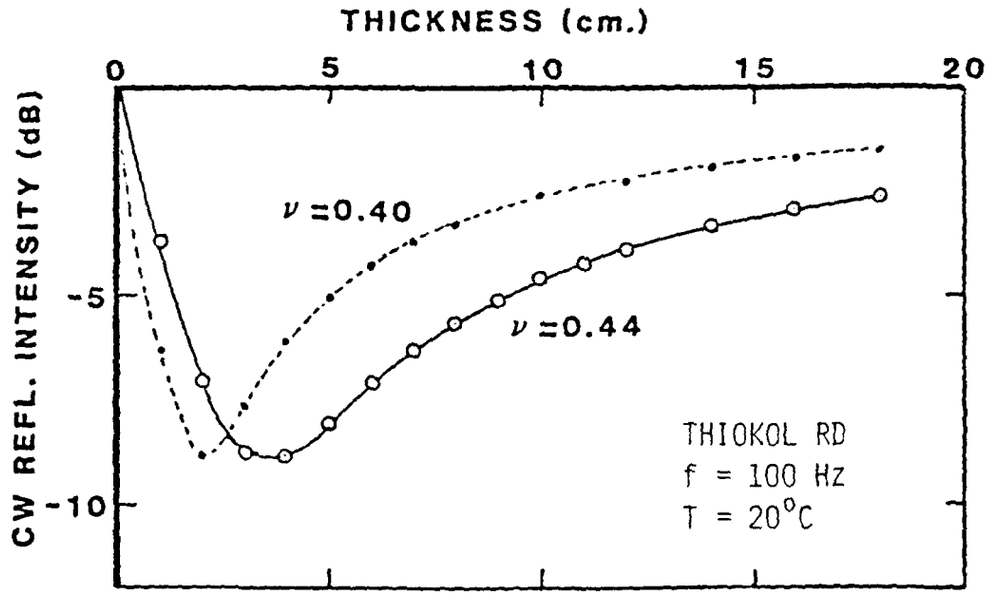

Figure 1-1. Calculated reflection reduction for Thiokol RD with $\nu = 0.40$ and 0.44 (from Gran, 1982)

* An experimental vibration damping elastomer developed in the 1940's and 50's which is no longer available.

1.2.2 Scope

This study effort consisted of four basic steps. The first step was the development of the theoretical background and basic algorithms to solve the problem of plane wave reflection reduction from a plane layer overlying a rigid perfect reflector. The second step involved obtaining material property data for available elastomers, running the algorithms with the data, and developing the final presentation format for the output data results. The third step was to analyze these computed results and parameter variations for the selected coating materials. The fourth and final step was the examination of application and analysis alternatives for underwater, low frequency target strength reduction.

The task of obtaining the "complete" low frequency, dynamic viscoelastic properties of available elastomers for the code calculations proved to be most difficult and time consuming. Although the dynamic properties of a wide variety of elastomers were available, the information for each individual elastomer was often incomplete. As a result, certain properties had to be estimated based on "typical" characteristics and values for elastomers. This required a more detailed study of viscoelasticity and an examination of the sensitivity of reflection reduction to these estimates by variation of these parameters.

1.3 Conclusions

After computing the acoustic reflection reduction capabilities of Thiokol RD (with reasonable estimates of its material properties) and three other representative elastomers, our conclusion is that for typical oceanic conditions (0°-30°C) and reasonable coating thicknesses (1-20 cm), the elastomers considered do not provide sufficient reflection reduction in the single homogeneous layer configuration for low frequency (order 100 Hz) acoustics. The reflection loss was, in all cases, no more than 6 dB for coating thicknesses less than 20 cm. The acoustic wavelength at 100 Hz in

the elastomer layer is about two orders of magnitude larger than a reasonable coating thickness. Therefore, unless the acoustic wavelength in the layer can be significantly reduced by reducing the sound speed in the layer, the effect of viscoelastic coatings having reasonable thicknesses on specular acoustic reflection should be negligible at low frequencies.

These conclusions do suggest that for effective low frequency, underwater anechoic coatings, the available elastomers might be modified to provide a lower coating sound speed. One technique for accomplishing this is by introducing inhomogeneities such as air voids, which convert energy from dilatational modes into shear modes for which the wave speed is much slower. Also, using such materials in coatings with a more complex geometry (layering and/or selective distribution about a body), significant target strength reduction may be achieved. Such an approach should include modal analysis which encompasses the total structure/coating system rather than just a simple geometric acoustic analysis since resonant interaction of the structure with the acoustic field may be just as dominant a mechanism at these low frequencies where the acoustic wavelength is on the order of the structure size.

1.4 Report Structure

The theory and analysis used to develop the algorithms for calculating the continuous wave reflection coefficient, the reflected impulse, and the reflection response to an arbitrary signal are discussed in Section 2. An examination of the relevant viscoelastic properties with respect to their frequency, temperature, and pressure dependence and their effect on acoustic absorption follows in Section 3. A parametric study of four representative elastomers is then presented in Section 4 in which the effects of coating thickness, temperature, density, and dynamic moduli are discussed. Lastly, observations, alternatives, application constraints, and a summary with recommendations for further analysis are given in Section 5.

2. THEORY AND IMPLEMENTATION

2.1 Assumptions and Conditions

The acoustic reflection algorithms were developed using the theory of geometric acoustics applied to plane acoustic waves incident on a plane, homogeneous layer overlying a rigid, perfect reflecting foundation (Figure 2-1).

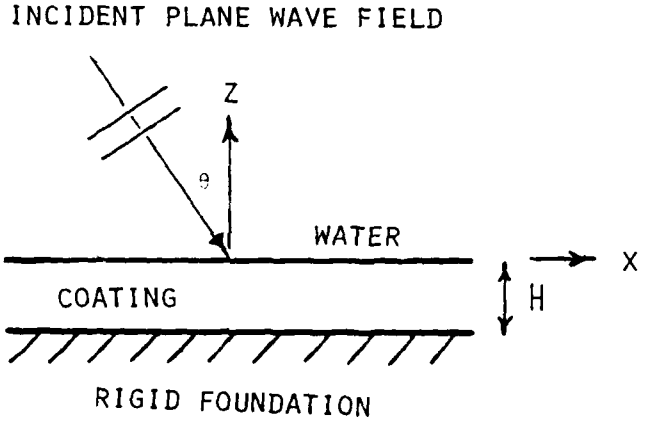

Figure 2-1. Coating geometry for the study

The assumption of an infinite plane layer neglects diffraction effects around a finite body, but since the acoustic wavelength and body size are within the geometrical scattering region, ($kr \gtrsim 2$) (Figure 2-2), and a coating has negligible effects on diffraction, the assumption is quite valid for this study of anechoic coatings.

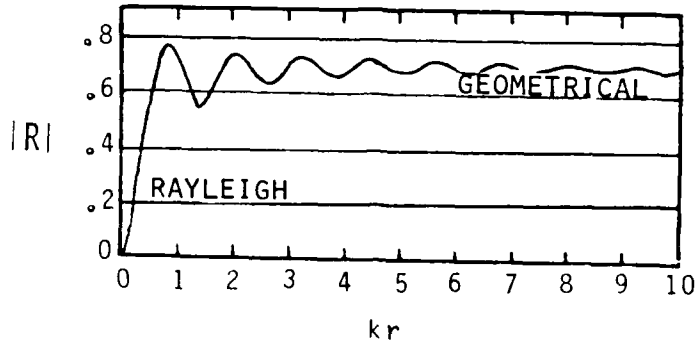

Figure 2-2. Scattering from a rigid cylinder with radius r (k = acoustic wavenumber) (adapted from Skudrzyk, 1971)

The plane layer represents an elastomer coating and the geometry results in the maximum specular reflection possible since the structure is approximated by a perfect reflector. Since only specular, monostatic backscatter is considered, only normally incident plane acoustic waves are of importance. As a result, only dilatational modes of wave propagation within the homogeneous plane layer will be considered since conversion to shear modes should be negligible at normal incidence.

2.2 Continuous Wave (CW) Reflection Coefficient

The plane wave (pressure amplitude) reflection coefficient for a plane viscoelastic layer overlying a perfect reflecting foundation is given by the equation

$$R = \frac{R_{12} + e^{-i2\phi}}{1 + R_{12}\, e^{-i2\phi}}$$

where

$\phi = H \frac{\omega}{c_1} D_2$ phase term

$R_{12} = \frac{D_1 - D_2}{D_1 + D_2}$ boundary reflection coefficient

$D_1 = \frac{\rho_2}{\rho_1} \cos\theta$

$D_2 = \sqrt{\left(\frac{c_1}{c_2}\right)^2 - \sin^2\theta}$

ω, θ acoustic frequency, incidence angle

ρ_1, c_1 fluid density and sound speed

H, ρ_2, c_2 layer thickness, density, and sound speed

A viscoelastic absorbing layer's sound speed (dilatational wave speed in this case) c_2 is complex, resulting in a complex reflection coefficient R, which accounts for absorption. A detailed formulation of the expression for R as a function of frequency, incidence angle, layer thickness, and material properties is given in Appendix A.

2.3 Reflected Impulse Response

The reflected impulse response is essentially the time series representation of the broadband reflection response of the coating. It is a compact representation summarizing the coating response over a large range of frequencies. Initially, the technique was considered to calculate the coating response to a very short (msec) duration pulse like that produced by a water gun which does not produce a CW signal (Figure 2-3). For long range propagation in which high frequencies are absorbed and deeper sources are utilized, the water gun (a cavitation device) cannot be used and signal pulses are of much longer duration (order tens of msec). In these long range applications, the CW (frequency) representation of the coating response is more relevant than the impulse (time) representation. The technique developed to obtain the impulse response from the CW results does provide a method of calculating the coating time response to an arbitrary pulse or signal whose transmitted spectrum is known.

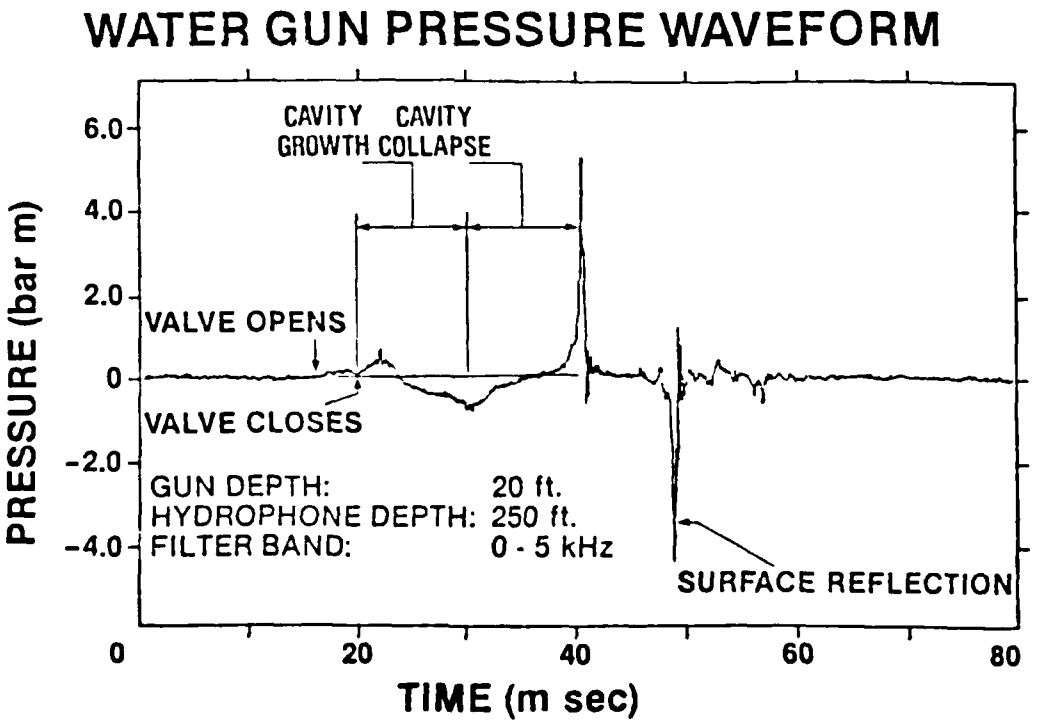

Figure 2-3. Water gun waveform (from Buoyoucos, *et al.*, 1980)

The plane layer reflected response as the ratio of the reflected pressure amplitude P_{refl} to the incident amplitude P_{inc} for an impulse (sudden on-off pulse of unit amplitude) is given by

$$\frac{P_{refl}}{P_{inc}} = I \doteq \frac{1}{2\omega_o} \int_{-\omega_o}^{+\omega_o} R(\omega)\, e^{i\omega\tau}\, d\omega$$

where ω_o frequency limit of $R(\omega)$ data

$\tau = \frac{1}{c_1}(x \sin\theta + z \cos\theta - c_1 t)$

$R(\omega)$ CW reflection coefficient as function of ω

$R(-\omega) = R^*(\omega)$ analytic continuation for negative frequencies

x, z distance along and distance from layer-water boundary

t time

Note that the finite frequency limit ω_o of the integral is an approximation of the exact impulse response (when $\omega_o = \infty$) since information on $R(\omega)$ at frequencies above ω_o is not included. The frequencies above ω_o are essentially "filtered" out of the incident and reflected impulse. In practice, the integral is evaluated by use of a discrete Fourier Transform (i.e., FFT algorithm) which represents a further approximation by replacing the integration with a discrete summation. A detailed formulation of the reflected impulse response expression is provided in Appendix A with a comparison of computation results with an exact solution showing good agreement.

2.4 Reflected Response to an Arbitrary Signal

The plane layer reflected response to an arbitrary waveform or a pulse-shaped acoustic signal can be computed by

$$I_s(\tau) \doteq \int_{-\omega_0}^{+\omega_0} S(\omega)\ R(\omega)\ e^{i\omega\tau}\ d\omega$$

where $R(\omega)$ is the complex CW reflection coefficient and $S(\omega)$ is the complex spectral decomposition (or Fourier Transform) of the incident signal. The spectral decomposition of an arbitrary transmitted signal can be obtained by various signal processing techniques (i.e., FFT) so that the reflected response of a plane layer to such an acoustic signal can be predicted with this technique. Essentially, the incident signal $S(\omega)$ is "modulated" by the plane layer response $R(\omega)$ resulting in the reflected signal response of the coating to an arbitrary incident signal. The inverse problem is also of interest in which a known transmitted incident signal $S(\omega)$ and reflected response $I_s(\tau)$ are measured to find the coating CW reflection response $R(\omega)$.

3. VISCOELASTIC PROPERTIES

3.1 Background and Assumptions

Viscoelasticity represents a class of material behavior between that of a viscous liquid and an elastic solid. The assumption of linear viscoelasticity is a good approximation of the behavior of most elastomers in typical stress-strain conditions. Linear viscoelasticity allows the modeling of stress-strain behavior by systems of linear viscous elements (dashpots) and linear elastic elements (springs) in series and parallel. For our application, the assumption of linear viscoelasticity applies, and the following discussion is based on such a concept.

3.2 Definitions and Relations

The single, most important material property of a viscoelastic layer in determining its effect on the reflection coefficient is the complex dilatational wave speed c of the elastomer material making up the coating layer, assuming negligible conversion into shear wave modes near normal incidence. The complex sound speed is dependent on the density and complex moduli of the material. This complex sound speed can be calculated from the other material properties by the standard relations

$$c^2 = \frac{M}{\rho} = \frac{\lambda + 2G}{\rho} = \frac{K + \frac{4}{3}G}{\rho} = \frac{2(1-\nu)G}{(1-2\nu)\rho}$$

where

ρ is the density

M is the complex longitudinal modulus

λ is the Lamé constant

G is the complex shear modulus

K is the complex bulk modulus

ν is Poisson's ratio

The complex moduli quantify the relationships for the magnitude and phase delay between stress and strain and, therefore, account for the speed and attenutation of sound in the material. Often, the term loss factor or loss tangent is introduced to describe the relation between the real and imaginary parts of a complex modulus. For example, the loss factor for the shear modulus is

$$\delta_G = \frac{G_i}{G_r} \quad \text{so that} \quad G = G_r\,(1 + i\delta_G)$$

where $G_r = Re\{G\}$ and $G_i = I_m\{G\}$. Unless the complex longitudinal modulus M is known, at least two other dynamic properties (i.e., ν and G, or K and G, etc.) must be known in order to calculate the complex sound speed c. The complex sound speed and attenuation are functions of frequency since the complex dynamic moduli of elastomers are functions of the frequency of stress loading.

3.3 Frequency Dependence

Usually, the available information on frequency dependent complex moduli for elastomers is in the form of the real part and the loss factor for the complex shear modulus G. For this reason, the frequency dependence of the dynamic shear modulus and its effect on sound absorption at different frequencies will be discussed. The shape of the complex dynamic shear modulus curve of viscoelastic materials as a function of frequency is quite general and can be represented by data for unvulcanized natural rubber (Figure 3-1).

The dynamic behavior of the elastomer can be separated into four different categories corresponding to the different frequency regions shown in Figure 3-1. At very low frequencies, viscoelastic materials behave more like viscous liquids in which deformation can continue at a fixed level of stress (i.e., creep), and viscous dissipation is the chief form of energy absorption. This type of behavior is characteristic of the "flow region".

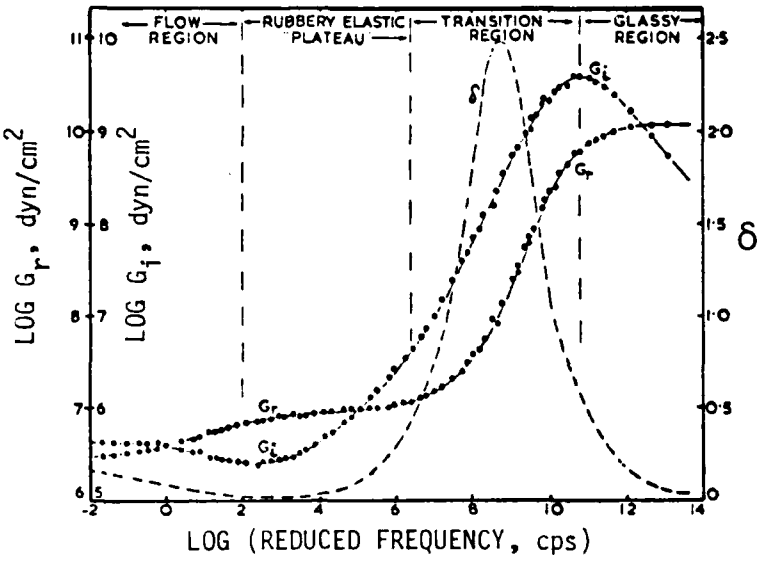

Figure 3-1. Dynamic shear modulus data (G_r = real part, G_i = imaginary part, $\delta = G_i/G_r$ loss factor) for unvulcanized natural rubber at 25°C (from Davey and Payne, 1964)

In the "rubbery elastic region" (at medium frequencies), elastomers behave in the rubber-like manner that we associate with these materials. In both the flow and rubbery elastic regions, the dynamic modulus remains relatively constant.

At higher frequencies, the dynamic behavior of elastomers passes through a "transition region" from a rubber-like behavior to a glass-like behavior. In this transition region, the complex modulus increases very rapidly with frequency, and the loss factor reaches a maximum. It is within this frequency range where the maximum absorption for the material occurs. At even higher frequencies above the transition region, elastomers behave in a glassy manner more like an elastic solid. In this "glassy region," the loss factor drops to very low values, and very little energy is absorbed by the material. The real part of the shear modulus G_r is nearly constant and approaches an asymptotic value at infinite frequency while the imaginary part G_i affecting absorption decreases.

3.4 Temperature and Pressure Dependence

For the range of operating pressures of interest in underwater coating applications (less than 500 psi), the sound speed of elastomers is relatively insensitive to changes in pressure (Figure 3-2). By comparison, for the range of operating temperatures 0°-30°C, the sound speed and dynamic moduli of elastomers change considerably more. The effect of temperature changes on the dynamic modulus of an elastomer is to shift the modulus vs. frequency curve in frequency while preserving its shape. In fact, dynamic modulus information can be represented by a master curve vs. reduced frequency ($a_T\omega$) at a reference temperature T_o and two empirical shift constants C_a and C_b. The amount that the modulus curve is shifted in frequency (a_T) to represent data at another temperature T is computed from the WLF (Williams, Landel, Ferry) equation (Ferry, 1980).

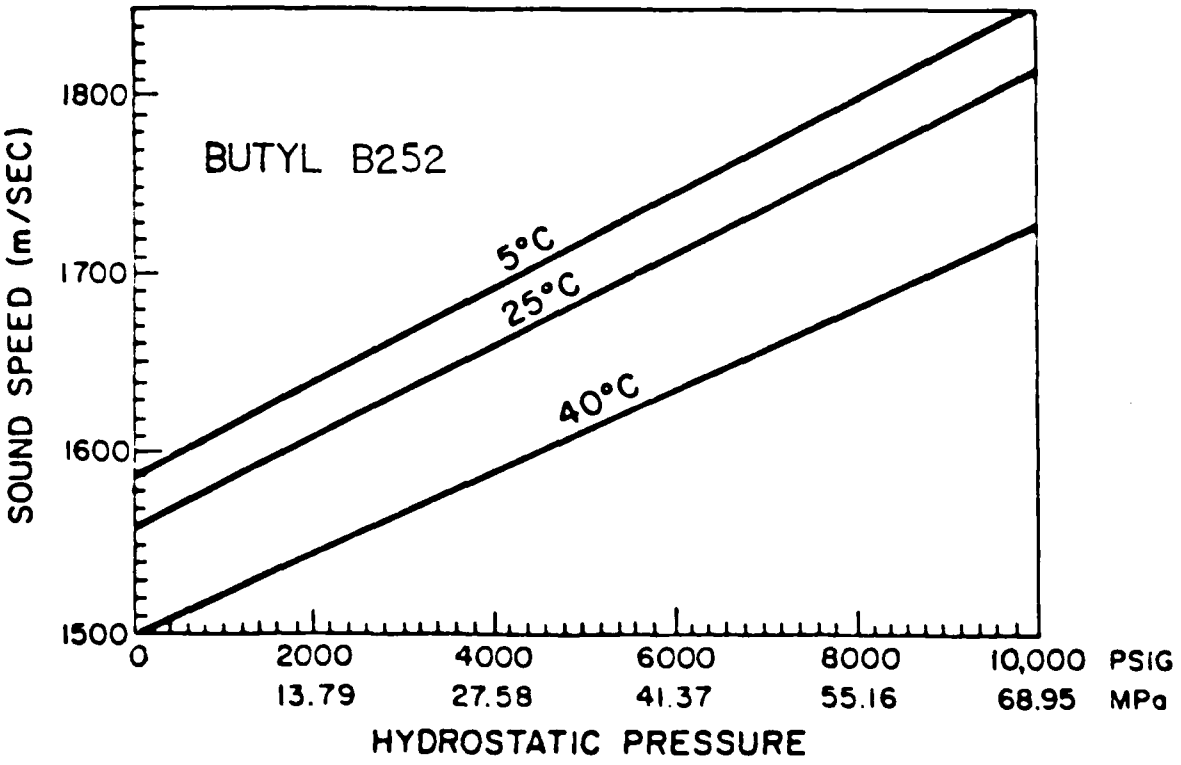

Figure 3-2. Pressure dependence of the sound speed (c_r) for Butyl B252 at three different temperatures (from Capps, Thompson and Weber, 1981)

$$\log a_T = \frac{C_a(T-T_o)}{C_b + (T-T_o)}$$

where the temperatures are in units of degrees Kelvin. Normally, an increase in temperature causes a shift of the modulus curve to higher frequencies while a decrease in temperature shifts the curve towards lower frequencies (Figure 3-3).

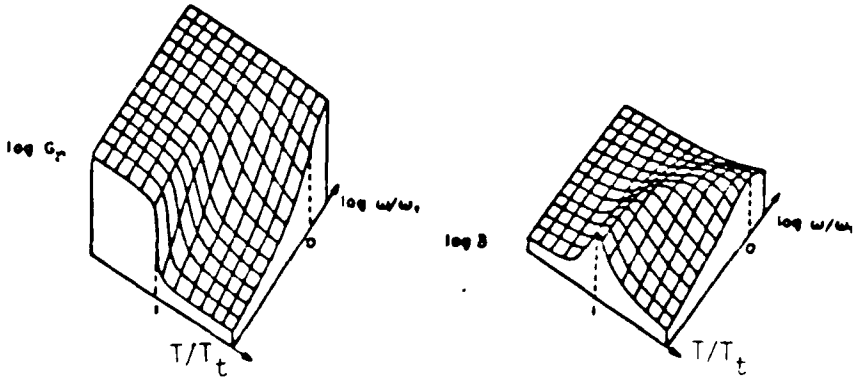

Figure 3-3. Temperature and frequency dependence of the dynamic shear modulus (G_r) and loss factor (δ) near the transition region where T_t and ω_t are the transition temperature and frequency (from Snowdon, 1968)

3.5 Classification of Elastomers

Elastomers can be classified as either high loss or low loss depending on the application, operating temperature and frequency range. Comparing the complex dynamic modulus information to classify a material as either high loss or low loss requires comparison of both loss factor and the real part of the dynamic modulus within the temperature and frequency range of interest. The fact that one elastomer has a higher loss factor than another is not sufficient to classify it as a higher loss material. In many cases, an elastomer with a higher loss factor than another can exhibit less damping and energy absorption.

For two elastomers with equal loss factors at a temperature and frequency of interest, the one with the lower value of the real part of the dynamic modulus will exhibit greater absorption and damping. In general, a low value of the real part of the dynamic modulus with a high value of loss factor results in greater damping and energy absorption (a high loss material). The complex modulus (both real part and loss factor) of the elastomers must be compared for the specific range of operating temperatures and frequencies since the behavior of some elastomers is extremely temperature and frequency sensitive.

The longitudinal modulus M is normally one to two orders of magnitude greater than the shear modulus G for viscoelastic (rubber-like) materials. This observation is exemplified by one's experience that rubber-like materials are much easier to bend (shear deformation) than to stretch (longitudinal deformation) and by the fact that shear waves exhibit much slower propagation speeds ($c_G = \sqrt{G/\rho}$) than dilatational waves in viscoelastic materials. For the temperature and frequency ranges of interest in this study (0°-30°C) and order 100 Hz acoustics, the common elastomers have values of the magnitude of the dynamic shear modulus on the order of 10^7 and 10^8 dyn/cm^2 while the magnitude of the dynamic longitudinal modulus is on the order of 10^9 to 10^{10} dyn/cm^2. In these operating conditions, the density and sound speed of these elastomers are nearly the same as water (ρ = 1.0 gm/cm^3 and c = 1.5 x 10^5 cm/s) so that their characteristic acoustic impedances (ρc) are well matched for application as underwater anechoic coatings (this is not true for applications in air in which the impedance mismatch is a major problem).

4. STUDY OF FOUR REPRESENTATIVE ELASTOMERS

4.1 Properties and Selection

Based on the high/low loss criteria discussed in the previous section and the availability of dynamic material property data, four specific elastomers were selected to study their effectiveness in low-frequency, underwater anechoic coating applications and their sensitivity to environmental and design changes (i.e., temperature and thickness). The four materials considered herein are Butyl B252, Neoprene W, Polybutadiene, and Thiokol RD. These were selected based on their low values of the real part of the dynamic shear modulus and high values of loss factor at frequencies on the order of 100 Hz in the temperature range 0°-30°C compared to other available elastomers.

The material property data used in this study were: density (ρ), real part of the dynamic shear modulus (G_r), shear loss factor (δ_G), and real part of the sound speed (c_r). In order to obtain longitudinal wave propagation information from the shear data provided (G_r, δ_G), it was necessary to assume a constant, real Poisson's ratio ν over the temperature and frequency range of interest. This assumption probably predicts more longitudinal absorption than is actually realized since it results in the longitudinal and shear loss factors being equal ($\delta_M = \delta_G$). At the low frequencies of interest here (order 100 Hz) the error introduced by this assumption should not affect our conclusions appreciably. Poisson's ratios for the elastomers were calculated from c_r, G_r, and ρ data using the relation

$$c_r^2 = \frac{2(1-\nu)G_r}{(1-2\nu)\rho}$$

assuming that $c_r^2 \gg c_i^2$ (which is reasonable at these frequencies). The results of these calculations are shown in Table 4-1. For elastomers, Poisson's ratio is typically in the range from 0.490 to 0.499. A reasonable estimate for Thiokol RD is then $\nu = 0.495$.

Table 4-1. Density (ρ), sound speed (c_r), and Poisson's ratio (ν) at T ≈ 10°C, f ≈ 10^2 Hz for the four elastomers examined

	ρ(gm/cm^3)	c_r(x 10^5 cm/s)	ν
Butyl B252	1.17	1.58	0.497
Neoprene W	1.44	1.60	0.499
Polybutadiene	1.13	1.40	0.498
Thiokol RD	1.25	1.13 *	0.495 *

* unknown, reasonable estimate

The master curves and WLF shift constants (C_a and C_b) for the dynamic shear modulus were available for Butyl B252, Neoprene W, and Polybutadiene (Roberts and Madigosky, 1980; and Capps, Weber and Thompson, 1981), but not for Thiokol RD. Data for Thiokol RD were available at three different temperatures (Snowdon, 1968) and were interpolated for 10°C. The different temperature curves then allowed calculation of the WLF constants for the master curve of Thiokol RD at 10°C. The dynamic shear modulus data for all four materials are shown in Figure 4-1 followed by their shear loss factors in Figure 4-2.

The dynamic longitudinal modulus data calculated from the results in Table 4-1 and Figure 4-1 using the relation

$$M = \frac{2(1-\nu)G}{(1-2\nu)}$$

are presented in Figure 4-3. The longitudinal wave speed used in the reflection algorithms can then be found from the relation

$$c = \sqrt{\frac{M}{\rho}}$$

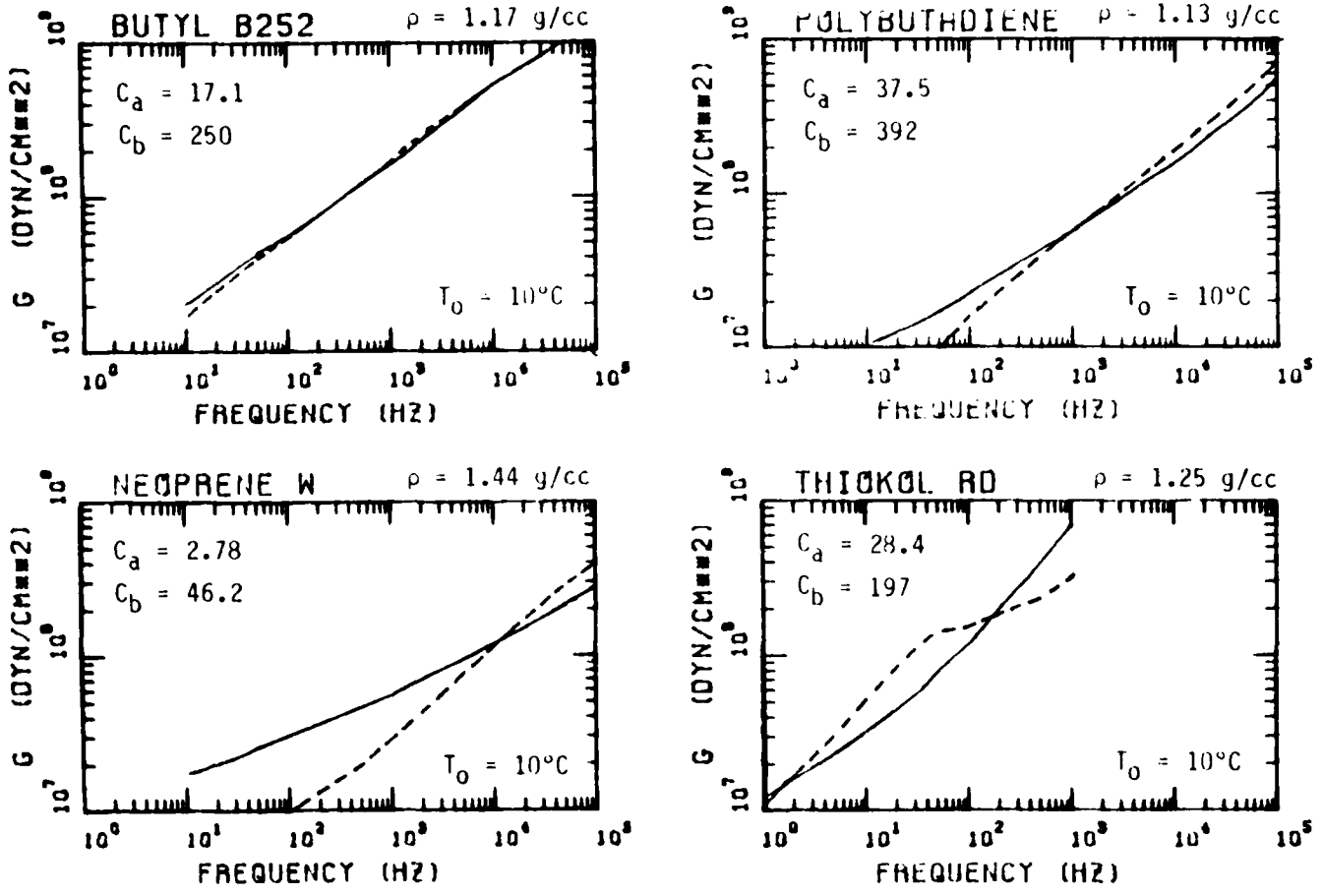

Figure 4-1. Master curves of the dynamic shear modulus G for Butyl B252, Neoprene W, Polybutadiene, and Thiokol RD at T_o = 10°C (——— real part G_r, ... imaginary part G_i)

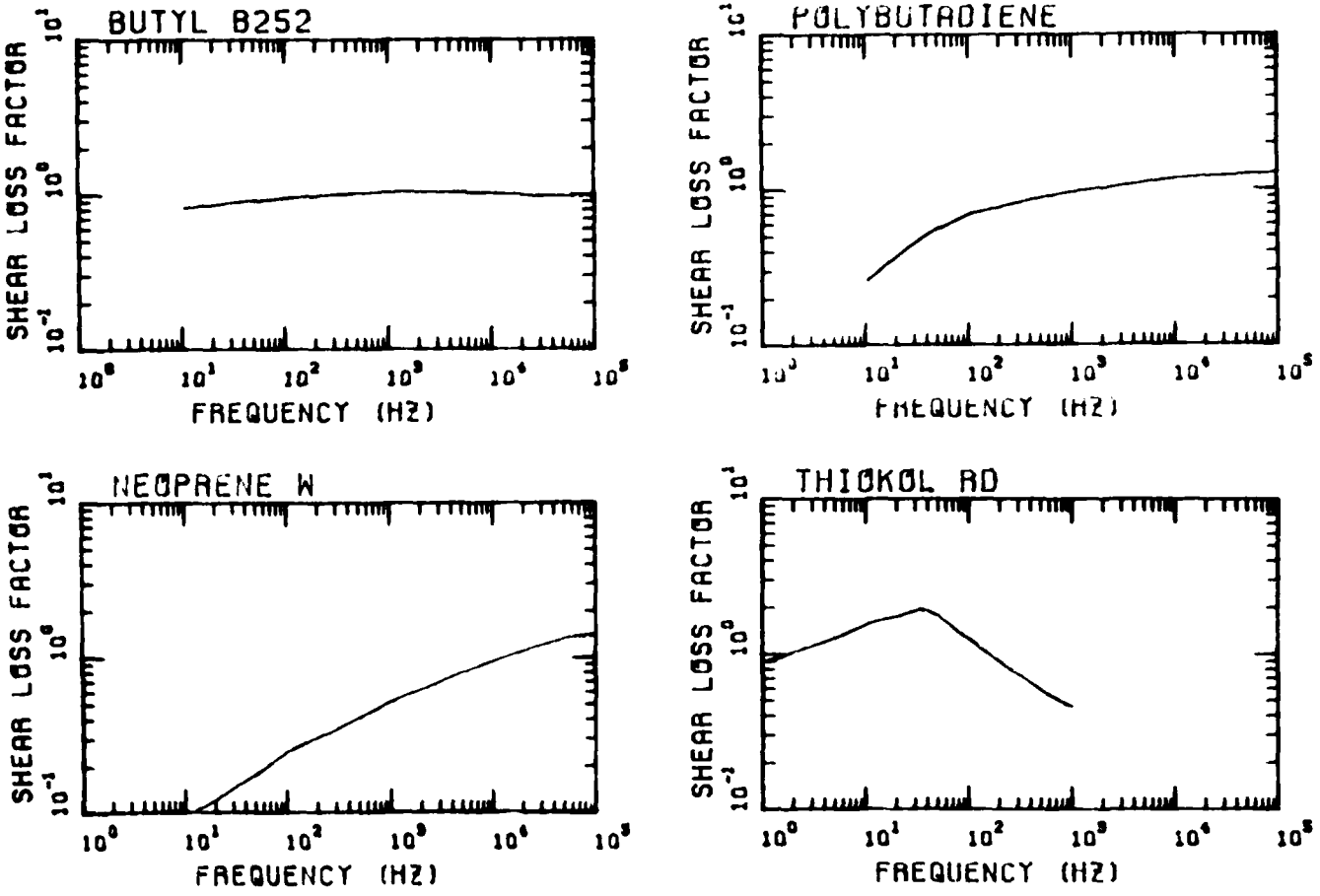

Figure 4-2. Shear loss factor δ_G for Butyl B252, Neoprene W, Polybutadiene and Thiokol RD at 10°C

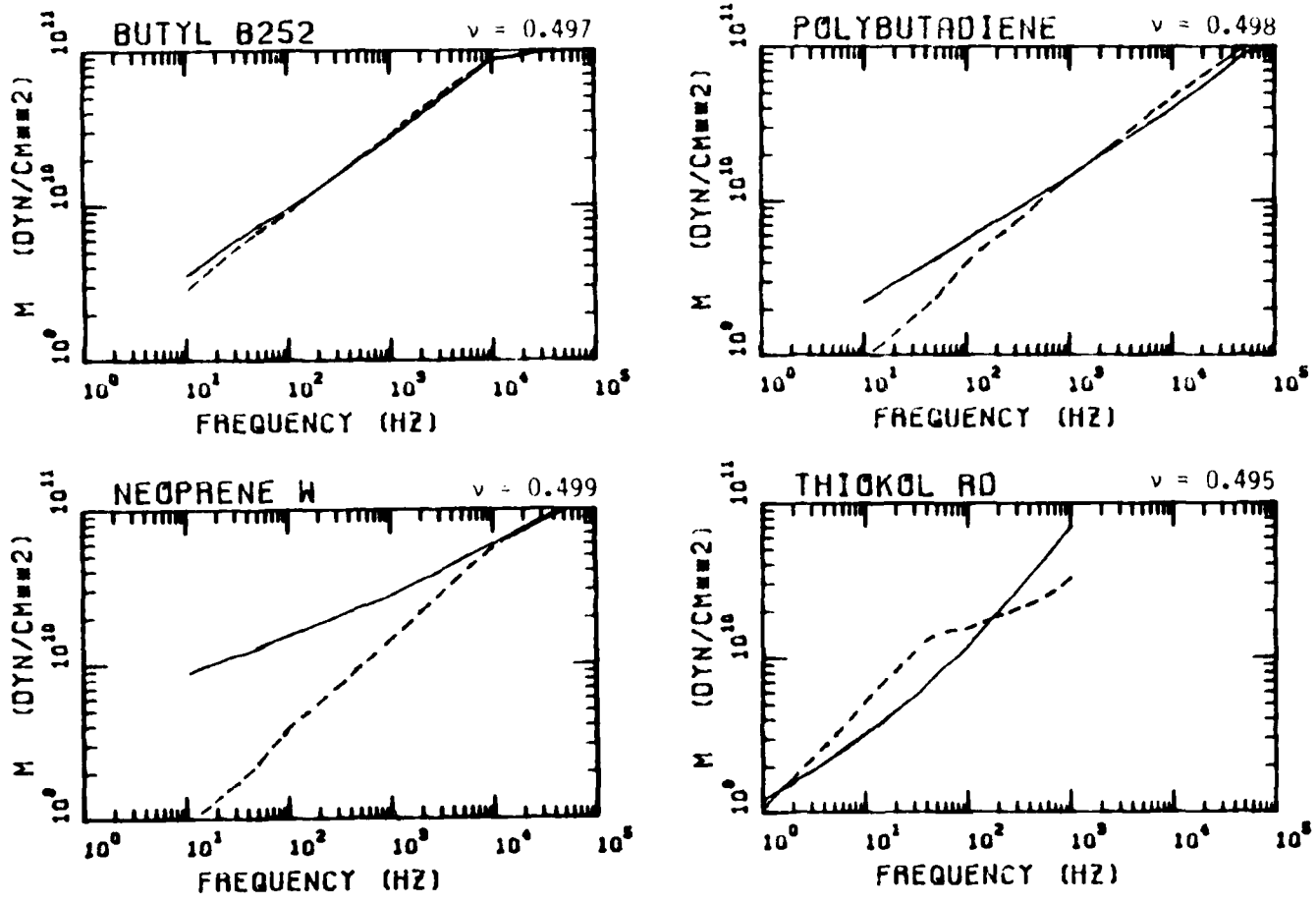

Figure 4-3. Calculated longitudinal modulus data (at 10°C) assuming constant, real Poisson's ratio ν and $\delta_M = \delta_G$ for the four selected elastomers used in computing reflection loss (——— real part M_r, — — — imaginary part M_i)

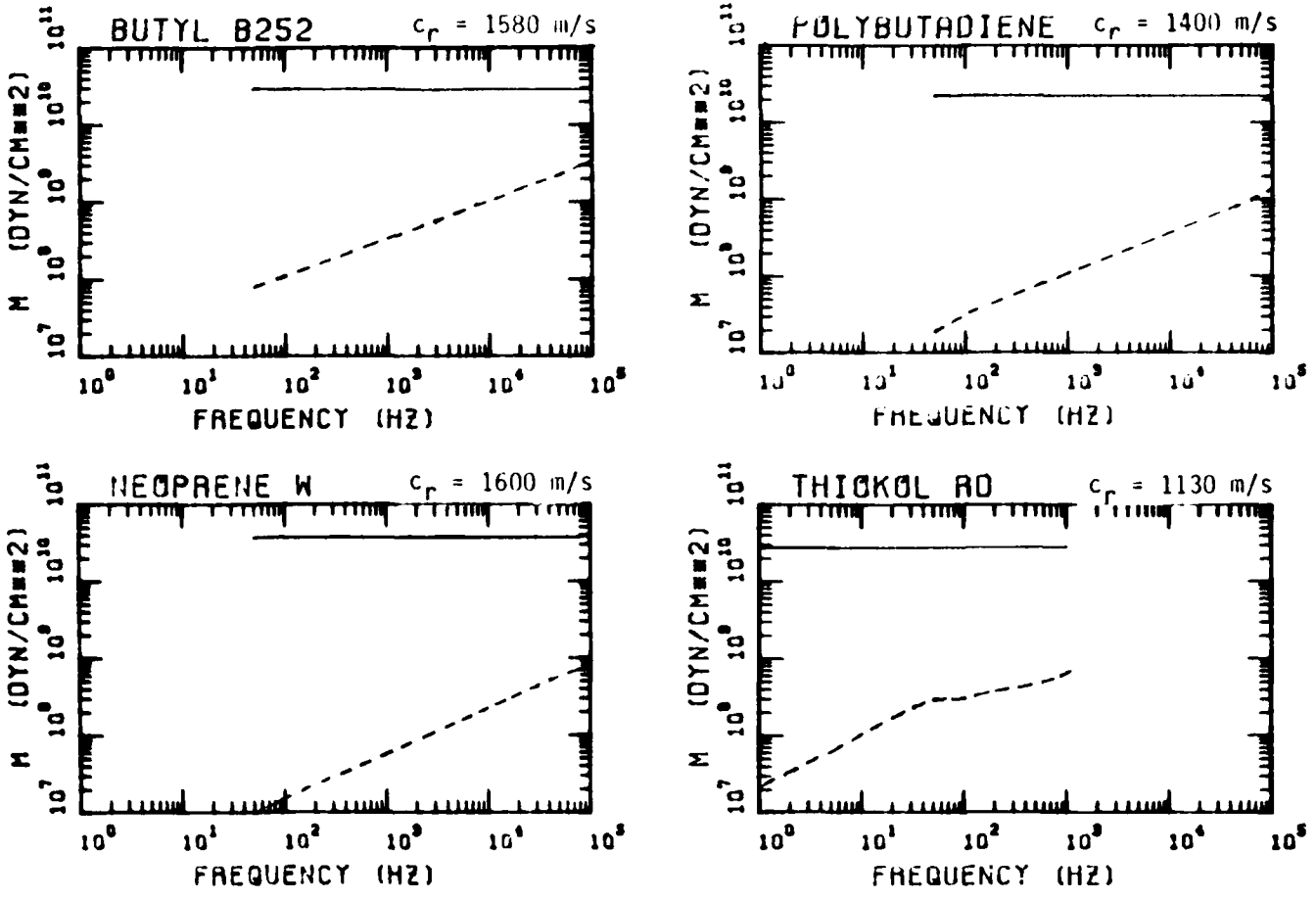

Figure 4-4. Calculated longitudinal modulus data assuming $\delta_M = 2\,\delta_G\,G_r/M_r$ ($\delta_M \ll \delta_G$) for the selected elastomers (——— real part M_r, – – – imaginary part M_i). Note unrealistic constant M_r curves

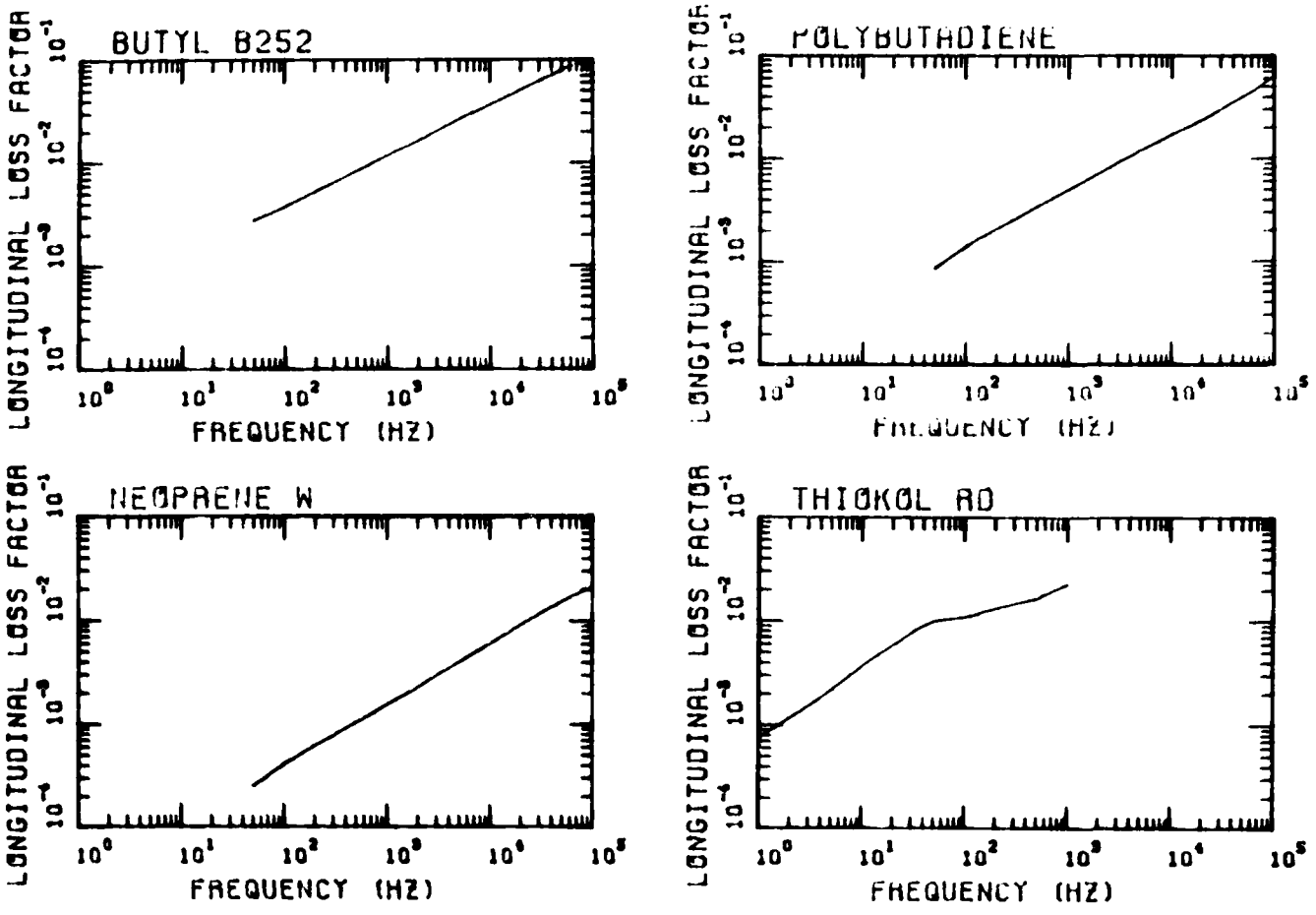

Figure 4-5. Calculated longitudinal loss factor δ_M for the data in Figure 4-4 resulting in negligible sound absorption ($\delta_M << 1$)

where both c and M are complex functions of frequency and temperature. Another expression relating shear properties to the longitudinal properties is given by

$$\delta_M = 2\,\delta_G \frac{G_r}{M_r}$$

(Madigosky and Fiorito, 1982) and results in substantially different values for the longitudinal moduli than the ones calculated by assuming a constant, real Poisson's ratio. This expression results from ultrasonic data on liquids and polymers and may not apply at the low frequencies in our case. Essentially this high-frequency expression results in negligible longitudinal absorption (reflection loss less than 1 dB) since M_r is about two orders of magnitude larger than G_r for elastomers. The longitudinal moduli were calculated using this ultrasonic-extrapolated expression and the results are displayed in Figure 4-4 followed by the calculated δ_M in Figure 4-5. The nearly constant value of M_r over frequency (Figure 4-4) leads us to believe that this ultrasonic extrapolation is not applicable to the present low frequency case since M_r should increase with frequency in this region. Therefore, the longitudinal data calculated using the constant, real Poisson's ratio assumptions (Figure 4-3) is used to compute reflection loss in this study and should be valid in the frequency range of interest.

4.2 Parameters and Conditions

For low frequency, underwater, anechoic coating applications the environmental and design parameters of interest are:

- acoustic frequency
- temperature
- pressure
- coating thickness.

Typical ranges of values for these parameters in this application are given in Table 4-2. The ambient water density and sound speed were taken as 1.0 gm/cm^3 and 1500 m/s, respectively, and the ambient pressure was set at 0 psig since the elastomers were found to be quite insensitive to pressure in the range of interest (Figure 3-2). The effects of temperature in the range 0°-30°C and coating thickness in the range 1-20 cm on effective coating reflection reduction at 100 Hz were examined in this study. The dynamic viscoelastic properties of the four elastomers examined at 100 Hz are tabulated in Table 4-3.

Table 4-2. Parameter value ranges of interest for underwater anechoic coating applications

acoustic frequency	order 100 Hz
temperature	0° - 30°C
pressure	0 - 500 psig
coating thickness	1 - 20 cm

Table 4-3. Dynamic modulus data for the four selected elastomers at 100 Hz for 10°C and 20°C.

	G_r (10^7 dyn/cm^2)		M_r (10^9 dyn/cm^2)		δ_G or δ_M	
	10°C	20°C	10°C	20°C	10°C	20°C
Butyl B252	5.7	2.9	9.6	4.9	0.96	0.88
Neoprene W	3.1	2.4	16.0	12.0	0.25	0.15
Polybutadiene	2.3	0.9	5.8	2.3	0.70	0.23
Thiokol RD	12.0	2.2	12.0	2.2	1.30	1.21

4.3 Reflection Loss Results

The reflection loss is defined as

$$RL = -10 \log |R|^2 \quad (dB)$$

where R is the complex CW pressure amplitude reflection coefficient discussed in Section 2.2. The lower limit of RL is 0 dB corresponding to total reflection of incident acoustic energy. The larger RL (in dB), the less acoustic energy is reflected and the greater the absorption by the coating. It is well to reiterate that the results presented are for specular backscatter from a plane, viscoelastic coating layer on a perfect reflecting, rigid half-space in water.

At 10°C, all four selected elastomers exhibit little reflection loss at frequencies below 1 kHz (Figure 4-6). Neoprene W and Thiokol RD exhibit the lowest calculated reflection losses at this temperature due to their high values of M_r (in spite of the relatively high value of δ_M for Thiokol RD; see Table 4-3). Polybutadiene exhibits the most reflection loss in this case because if has the lowest M_r of the selected materials at this temperature (Table 4-3).

At 20°C, the CW reflection loss results are quite different (Figure 4-7). Thiokol RD now exhibits the most reflection reduction since it has the lowest M_r and highest δ_M at this temperature (Table 4-3). The results for the other three elastomers are not significantly different from those at 10°C except that Butyl B252 now exhibits slightly more reflection loss than Polybutadiene in this case. At all temperatures of interest, Neoprene W gives the lowest reflection loss of the selected materials because it has a significantly higher M_r and lower δ_M.

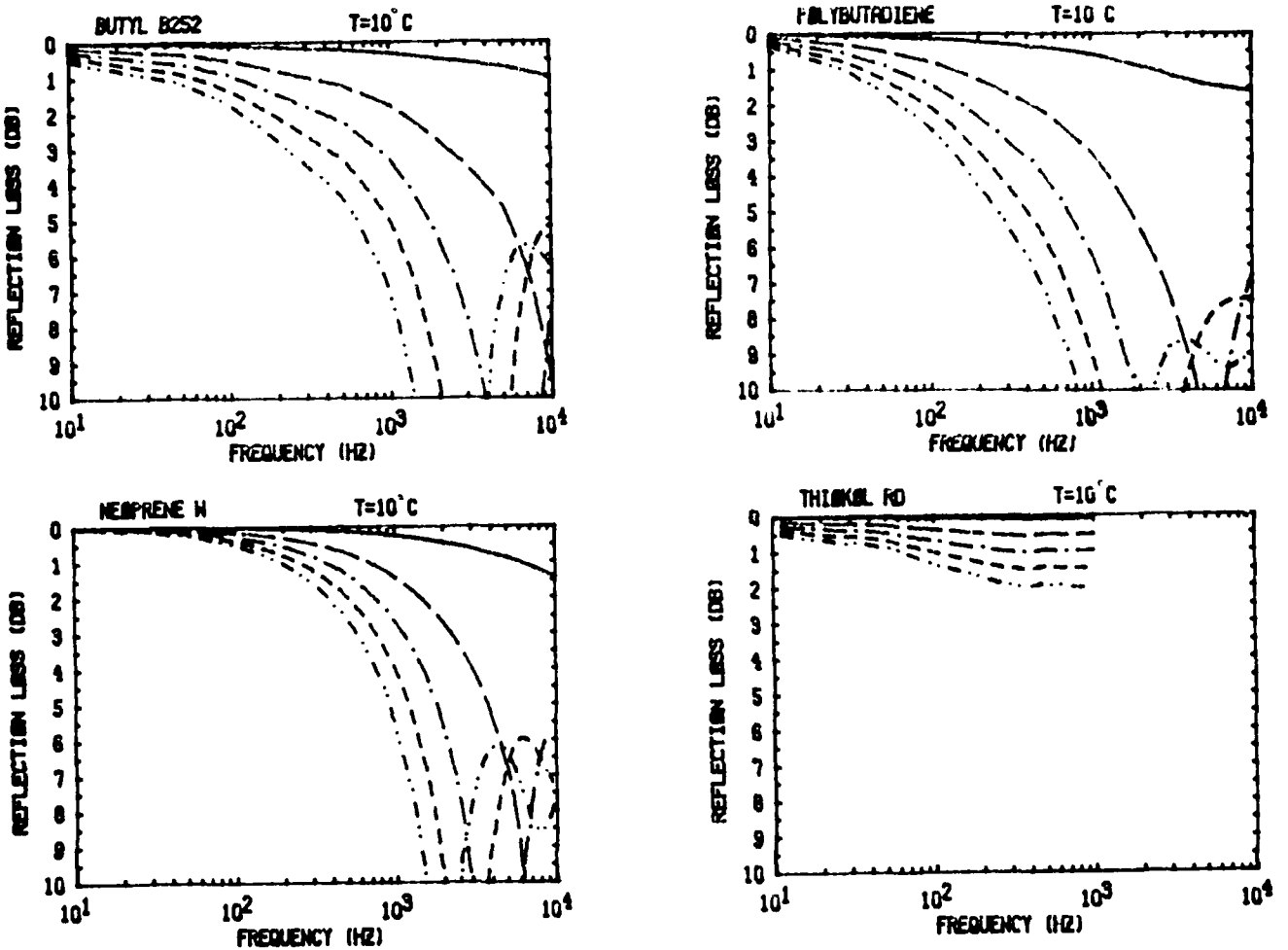

Figure 4-6. Calculated CW reflection loss for the selected elastomers at 10°C (——— 1 cm, — — — 6 cm, — . — 10 cm, — — — 15 cm, — .. — 20 cm)

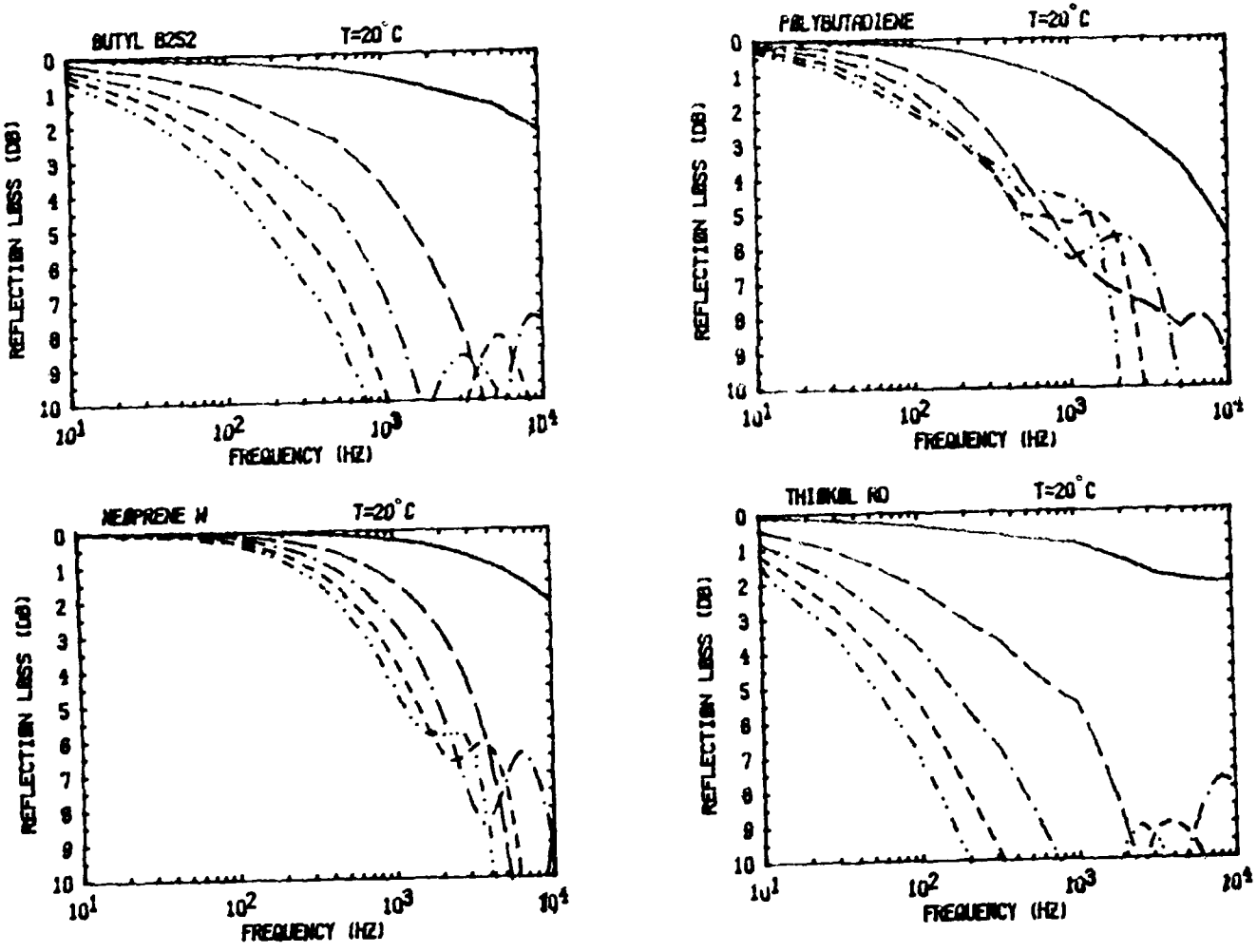

Figure 4-7. Calculated CW reflection loss for the selected elastomers at 20°C (——— 1 cm, — — — 6 cm, — . — 10 cm, — — — 15 cm, — .. — 20 cm)

Comparing the CW reflection loss results at the two temperatures (10°C and 20°C), it is apparent that the selected materials exhibit much greater reflection loss at high frequencies above 1 kHz (except for Thiokol RD at 10°C). In fact, maximum reflection reduction for these elastomers occurs in the neighborhood of 10 kHz corresponding to the quarter-wavelength thickness frequency in which the elastomer coating has a "optimum" thickness to maximize reflection loss. Also, Thiokol RD is extremely temperature sensitive, changing from a low loss elastomer at 10°C to a high loss elastomer at 20°C. The other three elastomers were relatively insensitive to temperature. Figure 4-8 displays the temperature and thickness dependence of coating reflection loss at 100 Hz for the four elastomers. It appears that Thiokol RD has an optimum coating thickness near 13 cm at 30°C while, at lower temperatures, the reflection loss increases with coating thickness. For Polybutadiene at 100 Hz, the optimum temperature is 10°C since the reflection reduction is less at both lower and higher temperatures (Figure 4-8).

Classifying the selected elastomers according to reflection loss at 100 Hz, Thiokol RD is a high loss elastomer at temperatures greater than 20°C and a low loss elastomer for temperatures below 10°C. Butyl B252 is a medium loss elastomer at 20°C and above and a low loss elastomer at 10°C and below. Both Polybutadiene and Neoprene W have very poor reflection reduction characteristics and can be classified as low loss elastomers. None of the elastomers provided more than about 6 dB of reflection reduction for coating thicknesses less than 20 cm (Figure 4-8).

The sensitivity of the calculated reflection loss to errors in the estimated Poisson's ratio ν is examined in Figure 4-9. Remember that Poisson's ratio for elastomers in these conditions is within the range from 0.490 to 0.499. As shown, reflection reduction is quite sensitive to Poisson's ratio. The sensitivity of reflection reduction to density was found to be negligible over the range from 1 gm/cm^3 to 2 gm/cm^3.

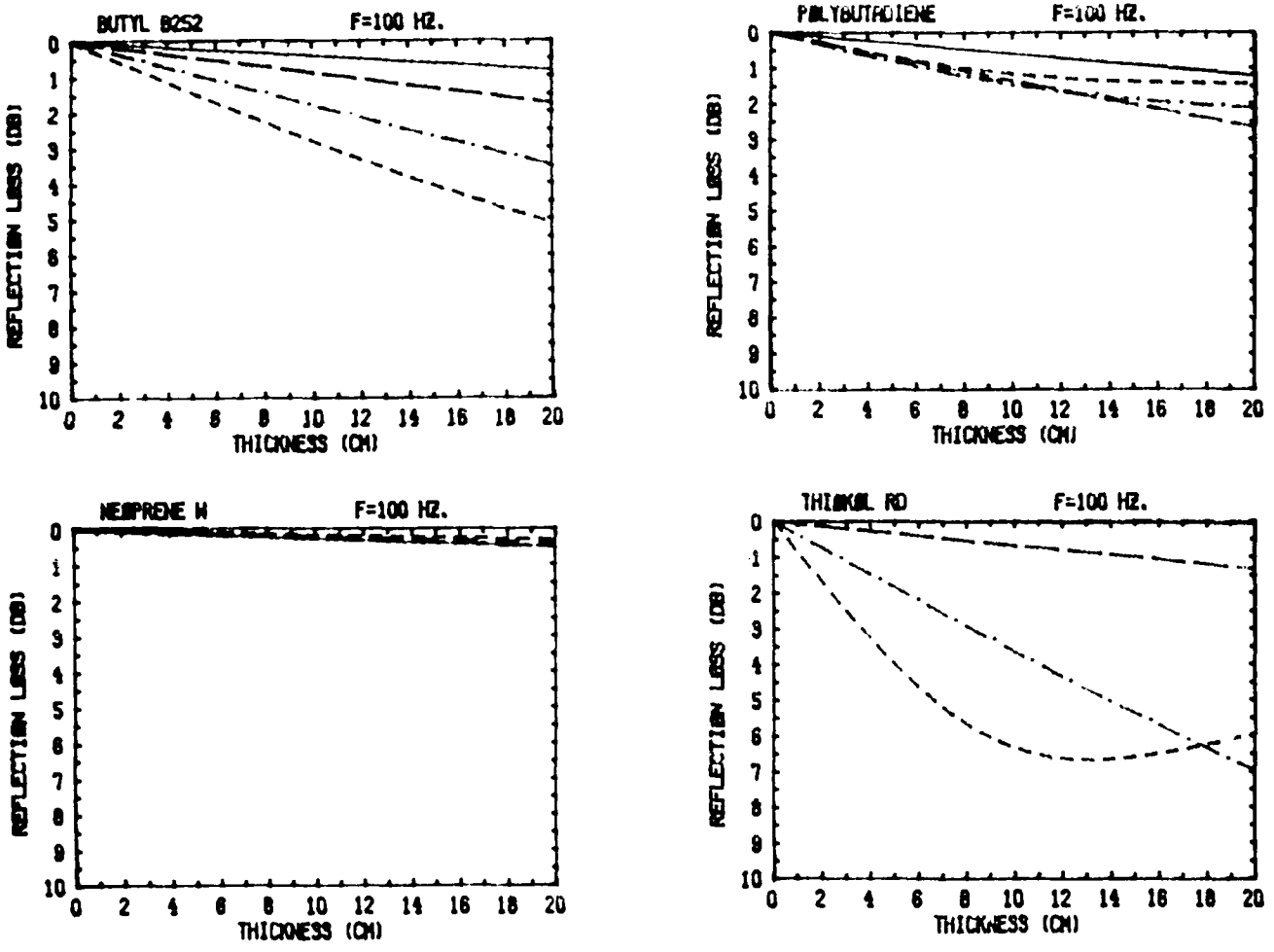

Figure 1-3. Calculated CW reflection loss for the selected ela tomers at 0°C (———) 10°C (— —), 20°C (— . —) and 30°C (– – –)

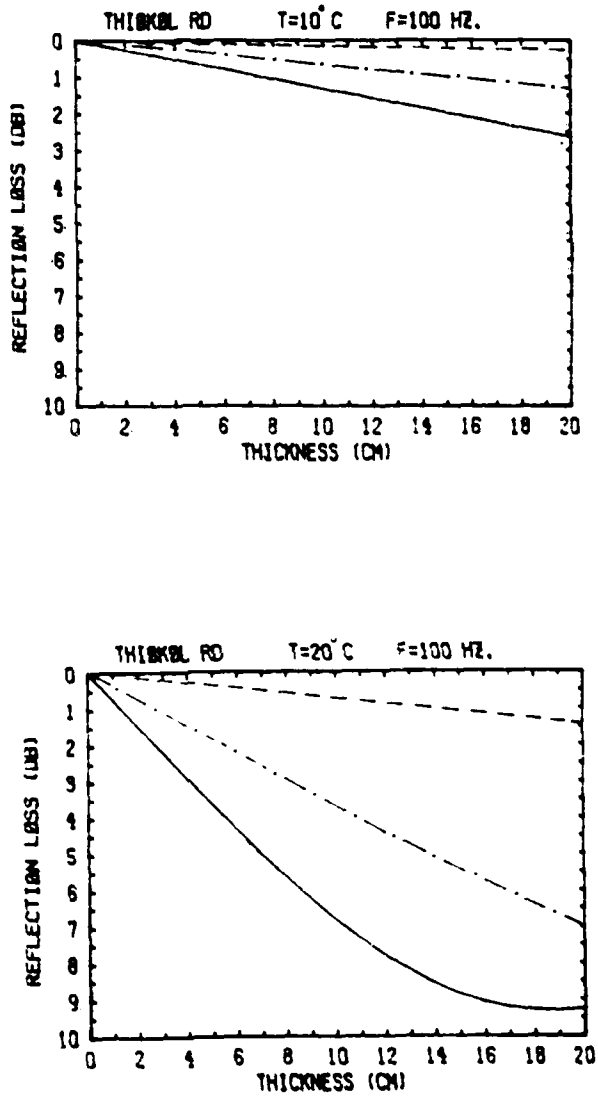

Figure 4-9. Sensitivity of calculated reflection loss to Poisson's ratio at 10°C and 20°C (— — — ν = 0.499, — . — ν = 0.495, ——— ν = 0.490) for Thiokol RD

4.4 Impulse Reflection Results

The reflection of an impulse (unit on-off pulse) from plane layers of the four selected elastomers at 10°C and 20°C was calculated using the complex pressure reflection coefficient vs. frequency results and the technique discussed in Section 2.3. The CW reflection coefficient (R) data covered frequencies up to 10 kHz, so for our calculations, the incident impulse (Figure 4-10) does not have energy at frequencies above 10 kHz. The impulse reflection results are then expressed as a pressure ratio (the ratio of reflected pressure to incident impulse pressure) vs. time (Figures 4-11 and 4-12) or time series of the reflected pulse.

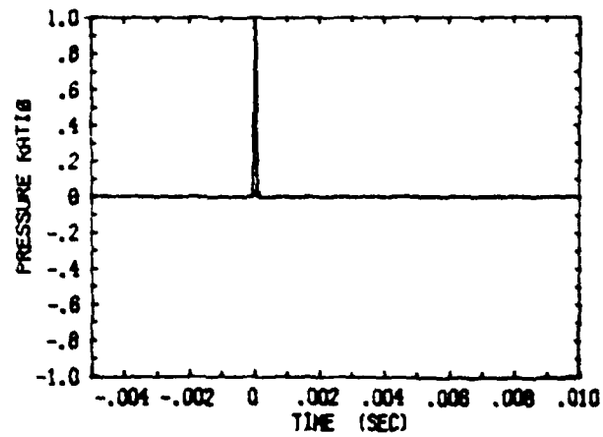

Figure 4-10. Incident unit impulse

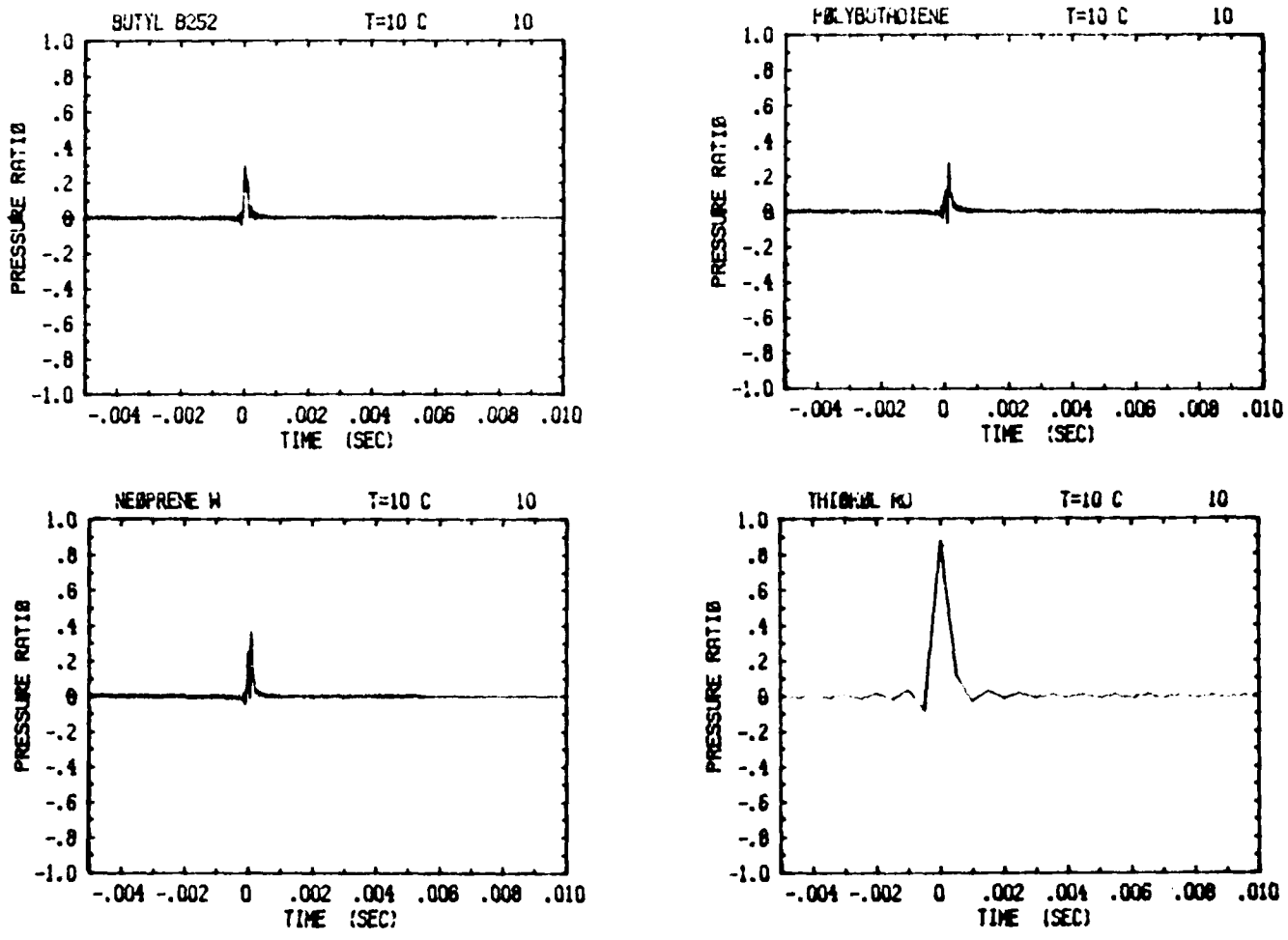

Figure 4-11. Calculated impulse reflection from a 10 cm layer of the selected elastomers at 10°C. The peak for Thiokol RD is wide due to FFT resolution (only components up to 1 kHz are included)

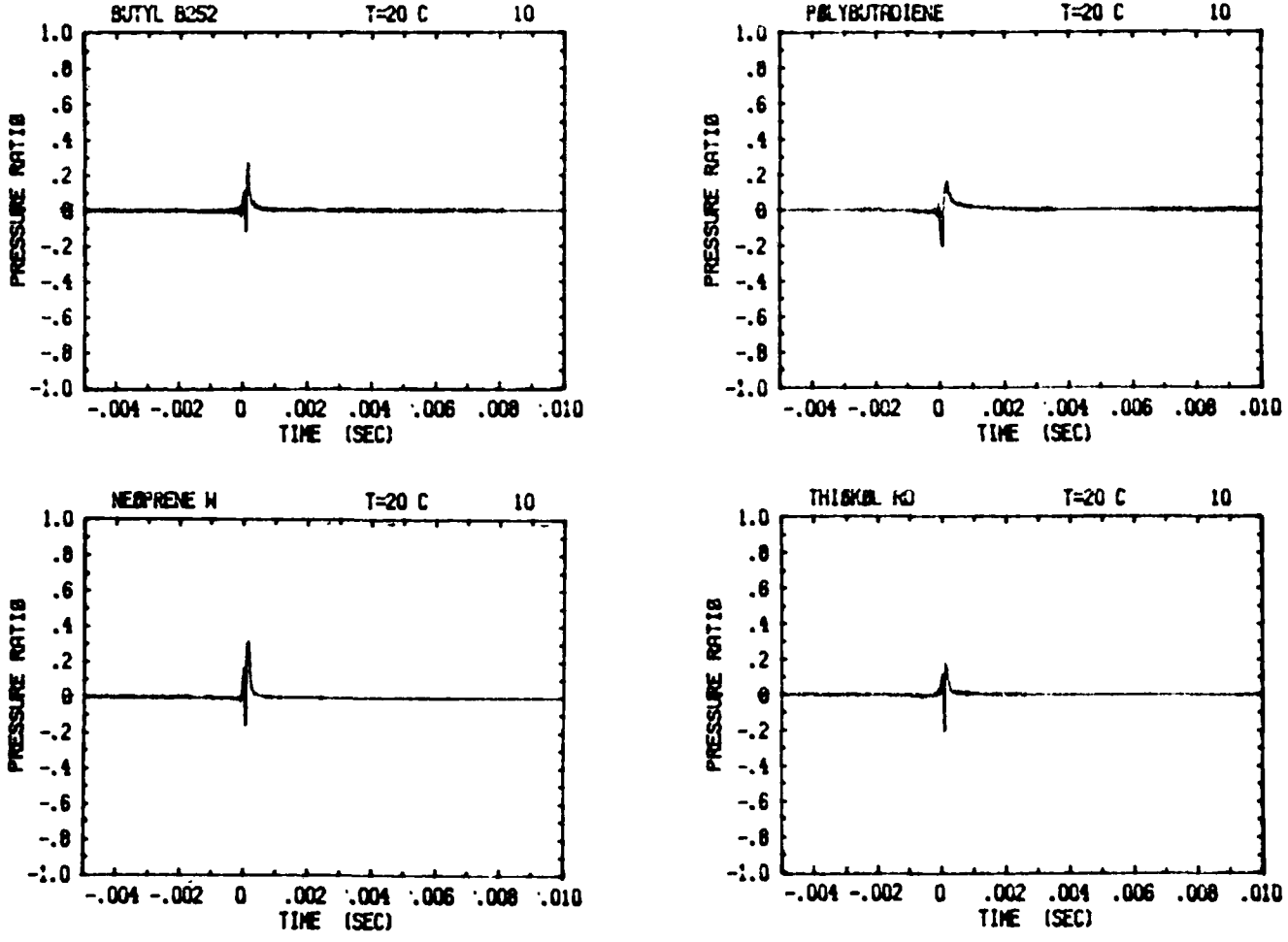

Figure 4-12. Calculated impulse reflection from a 10 cm layer of the selected elastomers at 20°C

Since the elastomers exhibit larger reflection reduction at frequencies above 1 kHz, the impulse reflection results are much better than for 100 Hz CW. The great difference between the results at 10°C and 20°C for Thiokol RD clearly demonstrates the large temperature sensitivity of its reflection response. The other three elastomers do not exhibit nearly as much temperature dependence in the impulse reflection results. Note that these results are for an ideal incident impulse (with frequency components above 10 kHz filtered out) rather than a realistic impulse which has some characteristic frequency and time width. The reflection of a realistic impulse or signal of arbitrary shape can be calculated using this technique (discussed in Section 2.4). These impulse reflection results provide a measure of the total broadband reflection response of a coating, and they exemplify the capability to calculate the coating time response to an arbitrary acoustic signal using this technique.

4.5 Limitations of the Study

The major limitation on the present study was the availability of elastomer dynamic properties. This limitation was overcome by combining available data to obtain reasonable estimates for the unknown material properties (i.e., Poisson's ratio) at the temperatures and frequencies of interest. Four elastomers were chosen to provide a cross-section of commonly available materials that might be used as anechoic coatings. Both Neoprene W and Polybutadiene represent low loss elastomers in our conditions. At temperatures above 20°C, Butyl B252 represents a medium loss elastomer, and Thiokol RD represents a high loss elastomer. At temperatures below 10°C all four elastomers can be considered low loss.

The dynamic material properties available were limited to frequencies up to 10 kHz (for the temperature range of interest) so the effects of absorption at higher frequencies are not considered. This is a good approximation for long range propagation in the ocean where high frequency acoustic wave components are attenuated significantly. Also, in oceanic applications at low

frequencies on the order of 100 Hz, the complete backscatter response of a coating on a structure whose size is on the order of an acoustical wavelength may not be accurately modeled by the response of an infinite plane layer because other backscatter mechanisms may be important. Instead, this study examines the reflection reduction effectiveness of various types of elastomers in the specular reflection backscatter regime. The plane layer reflection is a good measure of the specular reflection reduction of these elastomers for application in anechoic coatings regardless of structure size or shape. The study, therefore, is most useful for applications such as material selection where specular reflection reduction by a homogeneous coating is of primary concern.

5. DISCUSSION AND RECOMMENDATIONS

5.1 Alternatives and Options

From the results of this study, we find that elastomer coatings used in the simple homogeneous, single layer configuration do not provide significant low frequency acoustic, specular backscatter reduction for coating thicknesses of 20 cm or less in the ocean. At low frequencies (on the order of 100 Hz) in the ocean, the acoustic wavelength is two orders of magnitude larger than the typical coating thickness. Since the longitudinal wave speeds in the elastomers are almost the same as the sound speed in the water, the elastomer coatings are incapable of providing significant absorption at these wavelengths. In order to increase the absorption of incident acoustic energy, the acoustic wavelength within the coating can be reduced by mode conversion of longitudinal wave energy into shear wave energy for which the propagation speed is much slower. This effectively reduces the coating sound speed so the acoustic energy effectively "sees" more coating and absorption as it propagates at the slower speed.

One way to achieve a lower sound speed in the elastomer coating is to introduce inhomogeneities such as air voids which convert acoustic energy to shear modes of propagation. There is a trade-off involved in this approach. As the effective sound speed in the coating is reduced, the coating absorption capability is increased, but the impedance (ρc) mismatch between the water and coating is increased. This impedance mismatch causes a portion of the acoustic energy to be reflected directly from the water-coating interface without propagating (and being absorbed) in the coating. Further, such coating designs may be more sensitive to pressure changes. Clearly, there is some optimum coating density and sound speed that minimizes the total acoustic energy reflected from both the water-coating boundary and the propagation through the coating and reflection from the structure (Scharnhorst, 1979).

Multi-layer coatings may also help to reduce the impedance mismatch problem of introducing voids by matching the ρc impedance at the water-coating boundary and allowing a transition to lower sound speed and greater absorption. Such an approach has been examined at high frequencies (greater than 1 kHz) and found to be quite effective (Madigosky, 1981), but its effectiveness at low frequencies (below 1 kHz) is still in question. The high frequency, multi-layered, inhomogeneous elastomer coating approach relies chiefly on quarter wavelength attenuation within the layers to maximize reflection reduction. Comparable levels of anechoic effectiveness should not be expected at low frequencies since the layer sound speed would have to be reduced to about 100 m/sec or less for a 20 cm thick layer in order to take advantage of the quarter wavelength effect at 100 Hz.

Instead, at low frequencies, an analysis of the structure-coating system interaction with the acoustic field in the water may be more appropriate since the acoustic wavelength in water is on the order of the total structure size and specular reflection might not be the primary backscattering mechanism. In fact, resonant interaction of the coating-structure and the acoustic field may cause backscatter greater than that predicted by specular reflection alone (Gaunard, 1977). There are indications that at these acoustic wavelengths, the dominant mechanism for backscatter is not specular reflection but resonant structural vibration and reradiation by the structure (Gaunard and Kalnins, 1982). If this is the case, a modal analysis approach to examining the effects of low frequency coatings is more appropriate than the geometric acoustics approach of this study. The coating is then no longer an "anechoic" coating in the sense of reducing reflection, but serves more to modify the modal response of the structural vibration and reradiation.

5.2 Constraints for Underwater Applications

In the pressure range for underwater anechoic coating applications (0-500 psig), the common homogeneous elastomers are essentially insensitive to pressure changes. Instead, the primary sensitivity to depth changes is due to changes in seawater temperature (within the range 0°-30°C). The elastomers with broad transition regions and broad loss factor vs. frequency peaks tend to be less temperature sensitive than those with sharper loss factor vs. frequency peaks (i.e., Thiokol RD). This means that the elastomers which tend to be less temperature sensitive also tend to be less frequency sensitive and would be advantageous for undersea applications if they can provide significant reflection reduction. Unfortunately, the elastomers examined do not provide significant reflection loss at frequencies below 1 kHz throughout the range of application conditions.

If the coating thickness were not limited, sufficient anechoic response could be accomplished but only at much greater thicknesses than the range examined (1-20 cm). The permissible coating thickness is limited mainly by the coating density (buoyancy considerations) and hydrodynamic considerations. Most common elastomers have densities slightly greater than water, and if voids were introduced, their densities would decrease. If buoyancy was the only factor limiting coating thickness, very thick inhomogeneous (void) coatings would be permissible. The effects of the added bulk, mass, and compliance on hydrodynamic performance would have to be examined for such thick coatings. It appears doubtful that any available elastomer used as a homogeneous coating of the thickness considered would provide sufficient specular reflection reduction at low frequencies over the temperature range of interest. Thiokol RD does provide adequate reflection loss at 20°C and above, but it is extremely temperature sensitive and, therefore, not suitable for these applications unless the coating temperature can be maintained above 20°C (by utilizing waste heat from the vehicle's power plant, for example). If maintaining the coating temperature is considered, availability of sufficient thermal flux would have to be examined.

5.3 Summary and Recommendations

In summary, we have found that the commonly available elastomers are quite ineffective in reducing specular reflection at low frequencies (order 100 Hz) for the temperature range of interest (0°-30°C). Thiokol RD does provide adequate reflection loss if the coating temperature can be maintained above 20°C, perhaps by utilizing waste heat (from exhausted power plant cooling water). Introduction of more complex coating geometries, such as inhomogeneities and layering, may improve coating effectiveness in specular reflection reduction, but if the acoustic wavelength is on the order of the body size, resonant response of the whole structure system may be the dominant backscatter mechanism.

The geometric acoustics analysis used in this study for specular reflection reduction is not relevant to the case where structure vibrational response is the dominant backscattering mechanism. Instead, a modal analysis approach to the total structure vibrational response with consideration of coating, structure, and internal fluid properties, geometries, and coupling would be necessary. The major mechanism in reducing backscatter in this case would be vibration damping rather than coating absorption of incident acoustic energy as in the case of specular reflection reduction examined by this study.

REFERENCES

Borgiotti, G.V. (1981) *"Effectiveness of Acoustic Absorbers at Low Acoustic Frequencies,"* Inter-office Memo to J. C. Nolan, IDA.

Buoyoucos, J.V., McLaughlin, J.K., Jr. and Selsam, R.L. (1980), *"The HYDRO-SHOCK Water Gun,"* Paper at Soc. of Expl. Geophysicists, Tulsa, Oklahoma.

Capps, R.M., Weber, F.J. and Thompson, C.M. (1981) *"Handbook of Sonar Transducer Passive Materials,"* NRL Memorandum Report 4311.

Davey, A.B. and Payne, A.R. (1964) Rubber in Engineering Practice, Palmerton Publ. Co., N.Y., p. 36.

Ferry, J.D. (1980) Viscoelastic Properties of Polymers, 3rd ed., John Wiley & Sons, N.Y., pp. 264-290.

Gaunard, G.D. (1977) *"Sonar Cross Section of a Coated Hollow Cylinder in Water,"* Jour. Acoust. Soc. Am. 61(2):360-368.

Gaunard, G.D. and Kalnins (1982) *"Resonances in the Sonar Cross Sections of Coated Spherical Shells,"* Int. Jour. Solids Structures 18(12):1083-1102.

Gran, R.L. (1982) *"Low-Frequency Acoustic Absorbing Materials,"* Internal Memo to D.R.S. Ko and R. Chapkis, Dynamics Technology, Inc.

Madigosky, W.M. (1981) *"Development of a Broadband Anechoic Coating for Underwater Use (U),"* Proceedings of 34th Navy Symposium on Underwater Acoustics, Vol. IV (U), pp. 409-419.

Roberts, D.J. and Madigosky, W.M. (1980) *"Dynamic Viscoelastic Properties of Materials for Underwater Acoustic Applications, Part III,"* NSWC TR80-425.

Scharnhorst, K.P. (1979) *"Optimal Distribution of Density and Dilatation Modulus in Inhomogeneous Layers,"* Jour. Acoust. Soc. Am. 66(5):1526-1535.

Skudrzyk, E. (1971) The Foundations of Acoustics, Springer-Verlag, N.Y., p. 448.

Snowdon, J.C. (1968) Vibration and Shock in Damped Mechanical Systems, John Wiley & Sons, N.Y., p. 3.

APPENDIX A.

FORMULATION OF ACOUSTIC REFLECTION COEFFICIENT AND IMPULSE RESPONSE

A.1 Introduction

This Appendix summarizes part of the analysis needed to support the COAT project. Although the results were derived for COAT, they are quite general and applicable to many other problems. The general expression for the acoustic plane wave reflection coefficient of a plane layer is derived (using a wave number matching approach) and applied to a viscoelastic layer. The results of this derivation have been implemented in the FORTRAN code program COAT which calculates the total reflection coefficient as a function of layer thickness, incidence angle, frequency, and material properties (at a given temperature).

The layer (reflected) impulse response is then developed in general form and application to real problems of viscoelastic layers is discussed. The technique has been implemented in the FORTRAN program IMPULSE which uses the reflection coefficient data determined by COAT to calculate the impulse response for a viscoelastic layer. The results from IMPULSE are approximations of the actual response, and the effects of the finite FFT approximation used must be analyzed.

The results of applying the technique on an elastic layer are discussed in an example. The COAT program provides the reflection coefficient data needed as input into the IMPULSE program. The example shows excellent agreement with theoretical predictions for reflected pulse spacing and good agreement for the reflected pulse amplitudes accounting for corrections associated with the finite FFT technique.

A.2 Parameter List

Fluid:

density	ρ_1
sound speed	c_1

Viscoelastic Layer:

density	ρ_2
sound speed	c_2
thickness	H
dynamic shear modulus	μ
Poisson's ratio	ν
shear damping factor	δ
complex Young's modulus	E

Rigid (Base) Material:

density	ρ_3
sound speed	c_3

Acoustic Plane Wave:

wave number	$k=\omega/c$
radian frequency	ω
angle relative to boundary	θ

A.3 CW Reflection Coefficient

A general expression is derived for the plane wave (pressure) reflection coefficient of a plane layer separating two other media. This general reflection coefficient is expressed as a function of frequency ω incidence angle θ_1, and material properties (ρ_i,c_i). This general result is then applied to the case of a plane viscoelastic layer on a perfectly reflecting base material in water. The water is designated as medium 1, the viscoelastic layer as medium 2, and the base material as medium 3 (Figure A-1).

A.3.1 Derivation of the General Expression:

By examining the reflection and refraction of the plane wave at the two boundaries (12 and 23) between the three media (Figure A-1), the total plane wave reflection coefficient for the layer is found to be

$$R = R_{12} + T_{12}R_{23}T_{21}\, e^{-i2\phi} + T_{12}R_{23}R_{21}R_{23}T_{21}\, e^{-i4\phi} + \cdots$$

where R_{ij} = boundary reflection coefficient for pressure wave traveling from medium i towards medium j

T_{ij} = boundary transmission coefficient for pressure wave traveling from medium i to medium j

ϕ = $Hk_2 \cos\theta_2$ represents the phase shift in the layer of thickness H (where $k_2 \cos\theta_2$ is the vertical component of wavenumber in the layer).

Notice that the expression for R is in the form of a geometric series where

$$\sum_{n=0}^{\infty} r^n = (1-r)^{-1}$$

so that the total reflection coefficient becomes

$$R = R_{12} + T_{12} R_{23} e^{-i2\phi} \left[\sum_{n=0}^{\infty} (R_{21} R_{23} e^{-i2\phi})^n \right] T_{21}$$

$$= R_{12} + \frac{T_{12}R_{23}T_{21} e^{-i2\phi}}{1 - R_{21}R_{23}e^{-i2\phi}}$$

Since $T_{12}T_{21} = 1-R_{12}^2$ and $R_{12} = -R_{21}$, the expression is therefore

$$R = \frac{R_{12} + R_{23} e^{-i2\phi}}{1 + R_{12}R_{23} e^{-i2\phi}} .$$

This is the general expression for the plane wave (pressure) reflection coefficient of a plane layer separating two other media. R is a function of incidence angle θ_1, frequency ω, and material properties $(\rho_1,c_1,\rho_2,c_2,\rho_3,c_3)$ through the expressions for phase shift ϕ and boundary reflection coefficients R_{12} and R_{23} given

$$\phi = H \frac{\omega}{c_1} \sqrt{n_{12}^2 - \sin^2 \theta_1}$$

$$R_{ij} = \frac{m_{ij} \cos \theta_i - \sqrt{n_{ij}^2 - \sin^2\theta_i}}{m_{ij} \cos \theta_i + \sqrt{n_{ij}^2 - \sin^2 \theta_i}}$$

where H = layer thickness

$m_{ij} = \rho_j/\rho_i$ density ratio

$n_{ij} = c_i/c_j$ index of refraction

$i = 1,2$

$j = 2,3.$

A.3.2 Application To A Viscoelastic Layer

In the case of a viscoelastic layer on a rigid base material where $\rho_2 c_2/\rho_3 c_3 \ll 1$, $R_{23} \approx +1$ (hard boundary with no phase inversion on perfect reflection). For viscoelastic materials, the compressional wave (sound) speed c_2 is a function of material properties (which are dependent on frequency ω) such that

$$c_2 = \left[\frac{(1-\nu)\ E}{(1+\nu)(1-2\nu)\ \rho_2}\right]^{1/2}$$

(notice that since $c_2 = c_2(\omega)$, the material is dispersive). Therefore, for a viscoelastic layer separating water and a perfectly reflecting, rigid base material, the plane wave reflection coefficient becomes

$$R = \frac{R_{12} + e^{-i2\phi}}{1 + R_{12}\ e^{-i2\phi}}$$

where $\phi = H \frac{\omega}{c_1} D_2$ phase shift term

$$R_{12} = \frac{D_1 - D_2}{D_1 + D_2}$$ boundary reflection coefficient

$$D_1 = \frac{\rho_2}{\rho_1} \cos \theta_1$$

$$D_2 = \sqrt{\left(\frac{c_1}{c_2}\right)^2 - \sin^2 \theta_1}$$

$$c_2 = \left[\frac{(1-\nu)\, E}{(1+\nu)(1-2\nu)\rho_2}\right]^{1/2} \quad \text{compressional wave speed}$$

$$E = E_r (1+i\delta) \quad \text{complex Young's modulus}$$

$$E_r = 2\mu (1+\nu) \quad \text{real part of Young's modulus}$$

ν = constant — Poisson's ratio

$\mu = \mu(\omega)$ — dynamic shear modulus (real)

$\delta = \delta(\omega)$ — loss factor

(notice that R is complex and accounts for absorption and attenuation due to the viscoelastic layer).

A.4 Impulse Response

A general expression of the impulse (reflected) response of a plane layer for an incident plane acoustic impulse is derived using the CW reflection coefficient of the previous section. A method for finding this (reflected) response for viscoelastic layers in real conditions is then discussed.

A.4.1 General Impulse Response Integral

The incident pressure field of a harmonic plane wave of unit amplitude can be written

$$P_{inc} = e^{ik_1(x\sin\theta_1 - z\cos\theta_1) - i\omega t}$$

and the corresponding reflected field is

$$P_{refl} = R\, e^{ik_1(x\sin\theta_1 + z\cos\theta_1) - i\omega t}$$

(Figure A-2) where R is the total reflection coefficient (given in the previous section). The impulse response (general) is found by integrating the reflected field over all frequencies so that

$$I = \frac{1}{2\pi} \int_{-\infty}^{+\infty} R\, e^{ik_1(x\sin\theta_1 + z\cos\theta_1) - i\omega t} d\omega$$

and since $k_1 = \omega/c_1$, the response integral can be expressed as an inverse Fourier transform of the form

$$I(\tau) = \frac{1}{2\pi} \int_{-\infty}^{+\infty} R(\omega)\, e^{i\omega\tau} d\omega$$

where $R(\omega)$ = CW reflection coefficient (previous section)

$$\tau = \frac{1}{c_1}(x\sin\theta_1 + z\cos\theta_1 - c_1 t).$$

A.4.2 Solution For A Viscoelastic Layer

To solve the response integral $I(\tau)$ for actual material in real conditions, the FFT method appears to be the most efficient since an analytical solution is not probable due to the complex functional dependence of R on ω (described in the previous section). The frequency dependence of the layer material properties $\mu(\omega)$ and $\delta(\omega)$ are critical in determining whether or not the integral $I(\tau)$ is integrable in its present form and what minimum and maximum frequency limits are appropriate for the FFT to obtain an adequate approximation of the integral. Also, since the integration is taken from negative to positive frequencies, and the material properties are defined only for the positive frequencies, values of $R(\omega)$ must be extrapolated for negative frequencies.

In order to find the values of $R(\omega)$ for negative frequencies, the observation that (in reality) the impulse response is real only (not complex) is used to determine the even/odd characteristics of $R(\omega)$. The integrand of $I(\tau)$ is a complex expression

$$Re^{i\omega\tau} = Re\{Re^{i\omega\tau}\} + i\ Im\{Re^{i\omega\tau}\} .$$

For the integral $I(\tau)$ to be real only, $Im\{Re^{i\omega\tau}\}$ must be an odd function (whose integral from $-\infty$ to $+\infty$ is zero). Since $Re\{e^{i\omega\tau}\}$ is even and $IM\{e^{i\omega\tau}\}$ is odd, then $Re\{R\}$ must be an even function and $Im\{R\}$ must be an odd function. Therefore, the value of $R(\omega)$ for negative frequencies can be extrapolated from the results of $R(\omega)$ for positive frequencies by applying the knowledge that the real part of $R(\omega)$ is an even function and the imaginary part is an odd function. This can be expressed as

$$Re\{R(-\omega)\} = Re\{R(\omega)\} \quad \text{even}$$

$$Im\{R(-\omega)\} = -Im\{R(\omega)\} \quad \text{odd}$$

or $$R(-\omega) = R^{*}(\omega)$$

where the * superscript denotes the complex conjugate.

The minimum and maximum frequency limits for the FFT are determined by the material properties data available. Extrapolation of the material properties data beyond the frequencies for which they are available (when greater accuracy in the impulse calculation is needed) can be based on experimental observations and a physical understanding of the important processes. The effect of approximating the impulse response integral with a finite FFT must still be determined. The correction coefficient for the reflected response to a unit amplitude impulse is dependent on the frequency limits used in the finite FFT approximation.

A.5 Application of Technique

The technique of calculating the reflection coefficient (from material properties) and the reflected impulse response of a plane layer has been applied to the case of an elastic layer for which the exact theoretical solution is tractable. In this way, the technique, discussed in the previous sections, can be compared with the exact solution to find the degree to which this finite FFT technique approximates the expected reflected response.

The programs COAT and IMPULSE have been tested for a 10 cm thick elastic layer with $E = 2.88 \times 10^8$ dynes/cm^2 and $\nu = 0.44$ for a unit impulse at normal incidence. The density of the layer was taken to be twice that of the first medium ($\rho_2/\rho_1 = 2$). The results (calculated by COAT) for the real and imaginary parts of R (the reflection coefficient of the layer) as a function of frequency (up to 10^4 Hz) are plotted in Figure A-3. The reflected response to a unit impulse (calculated by IMPULSE) is plotted in Figure A-4. The FFT size was 2048 (for a full frequency range of 10^8 Hz) with cosine tapering of 10% on each end.

The exact theoretical prediction for this normal incidence case is given in Figure A-5. The theoretical prediction gives a reflected pulse spacing of about 1 msec and reflected pulse amplitudes (ratios of reflected and incident amplitude) of -0.561, 0.685, 0.384, 0.216, 0.121, 0.068, 0.038, etc., respectively. Comparing the expected (theoretical) result with the IMPULSE calculation (Figure A-4), we see that the (IMPULSE) technique correctly predicts the pulse spacing and closely approximates the amplitudes of the odd pulses, but the even pulses (starting with the first positive pulse) show much less agreement in amplitude. Increasing the size of the FFT (the frequency resolution of the data) did not significantly affect this discrepancy between odd and even pulse amplitude approximations, but increasing the frequency range (and limit of the FFT) up to 10^5 Hz eliminated this discrepancy at the expense of increasing the error for the odd pulses (Figure A-6).

The results of this example indicate the effects of approximating the impulse response integral with the finite FFT technique and possible methods of correcting for the discrepancy (i.e., increasing the frequency limits to reduce the odd/even pulse error). The COAT/IMPULSE technique is shown to be a good predictor of the expected (actual) reflected impulse response given the geometry and material properties of the layer of interest.

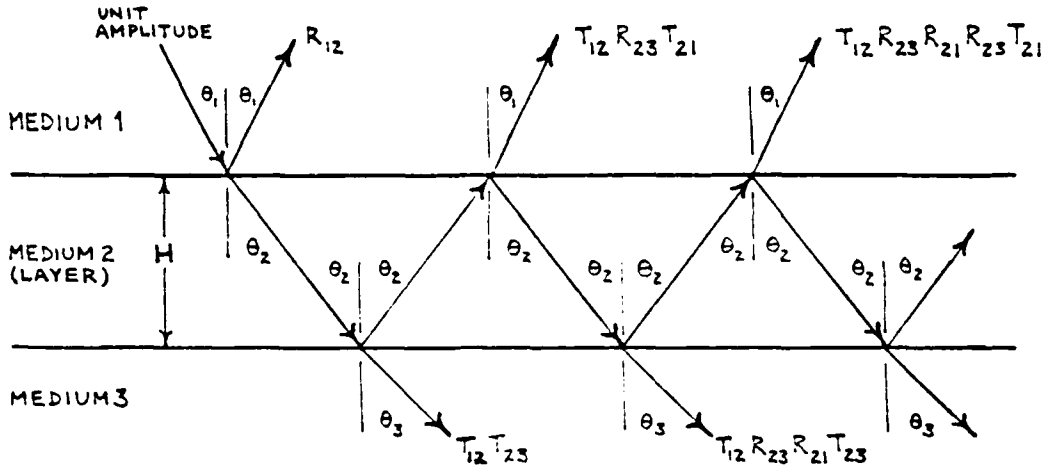

Figure A-1. Plane layer (plane wave) reflection.

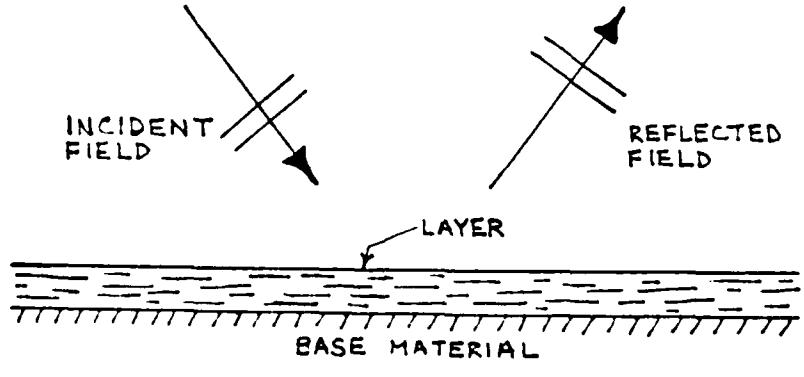

Figure A-2. Schematic of plane layer total reflected layer.

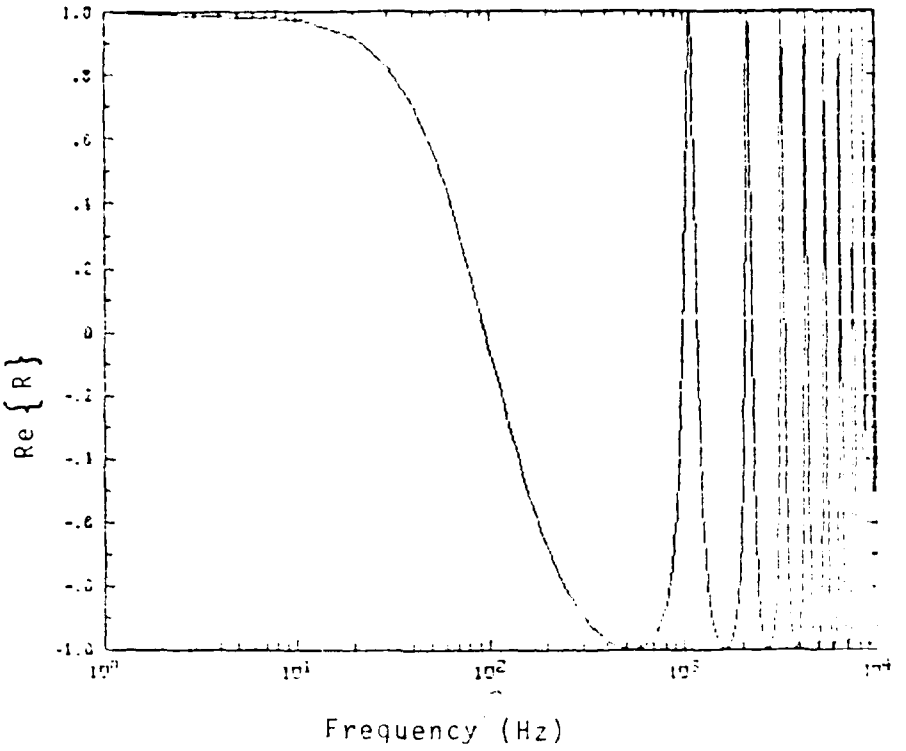

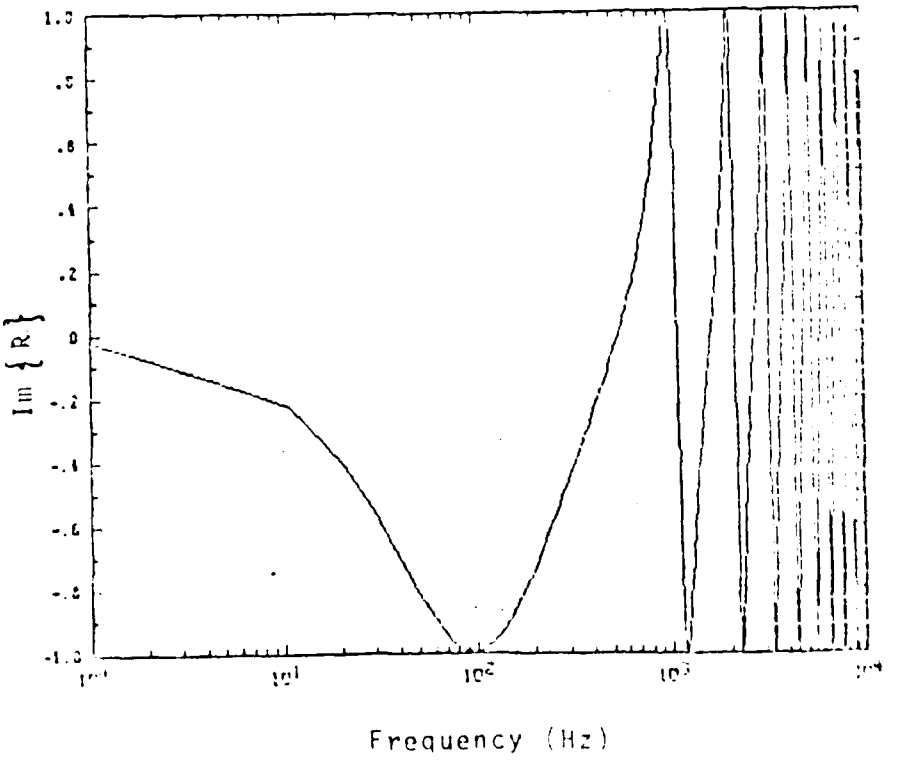

Figure A-3. Frequency dependence of reflection coefficient.

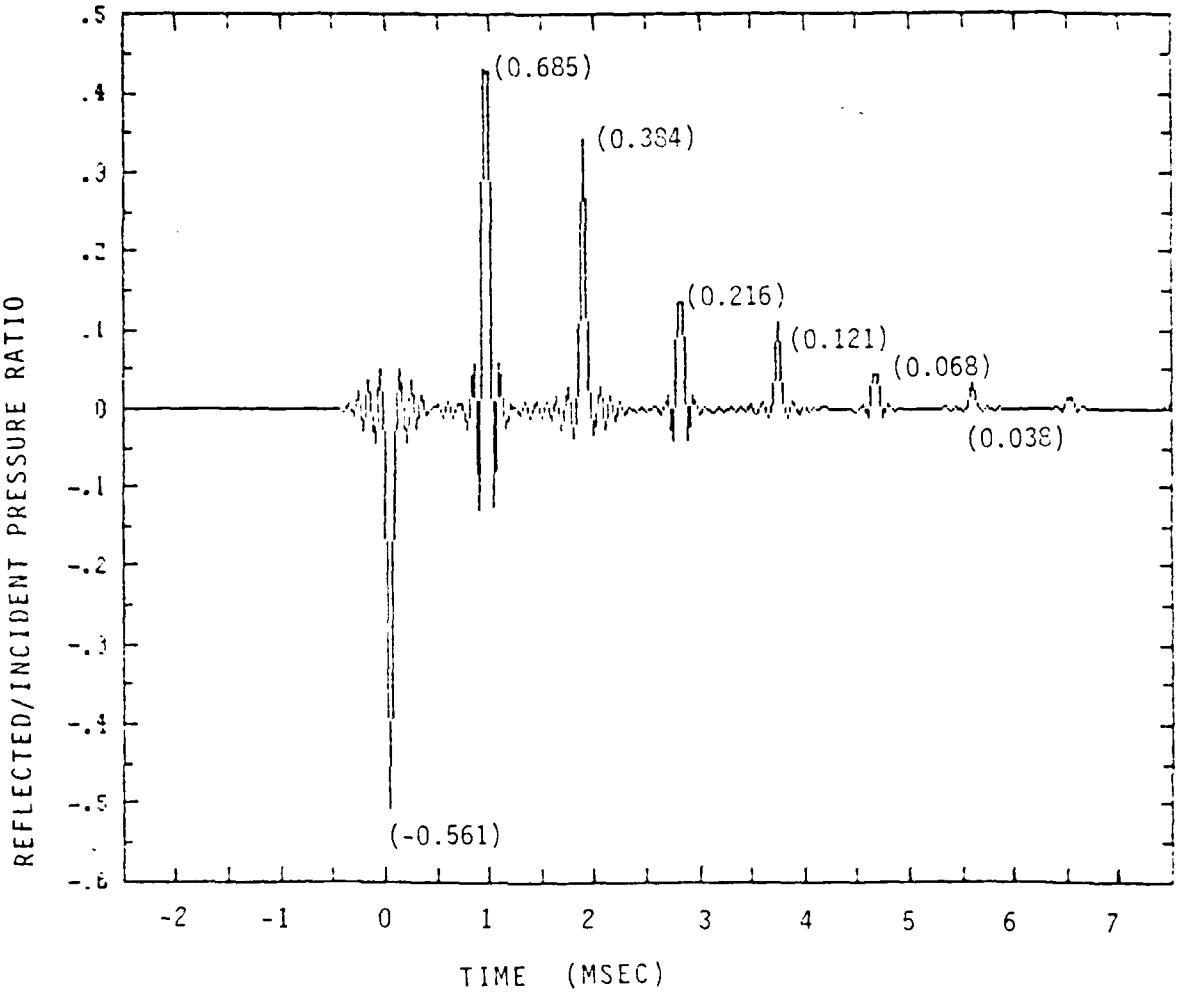

*theoretically predicted reflection impulse amplitudes are shown in parentheses.

Figure A-4. Reflected impulse response of layer calculated using the finite FFT technique on the reflection coefficient result in Figure A-3.

medium 1 $\rho_1 = 1$ $c_1 = 1.5 \times 10^5$

medium 2 $\rho_2 = 2$ $c_2 = \sqrt{\frac{(1-\nu)E}{(1+\nu)(1-2\nu)\rho_2}} = 2.16 \times 10^4$

*units are in cgs system

$$m_{ij} = \frac{\rho_j}{\rho_i} \qquad n_{ij} = \frac{c_i}{c_j}$$

$$R_{ij} = \frac{m_{ij} - n_{ij}}{m_{ij} + n_{ij}} \qquad T_{ij} = \frac{\rho_i}{\rho_j}(1 + R_{ij})$$

$R_{12} = -0.561$ $T_{12} = 0.225$

$R_{21} = +0.561$ $T_{21} = 3.046$

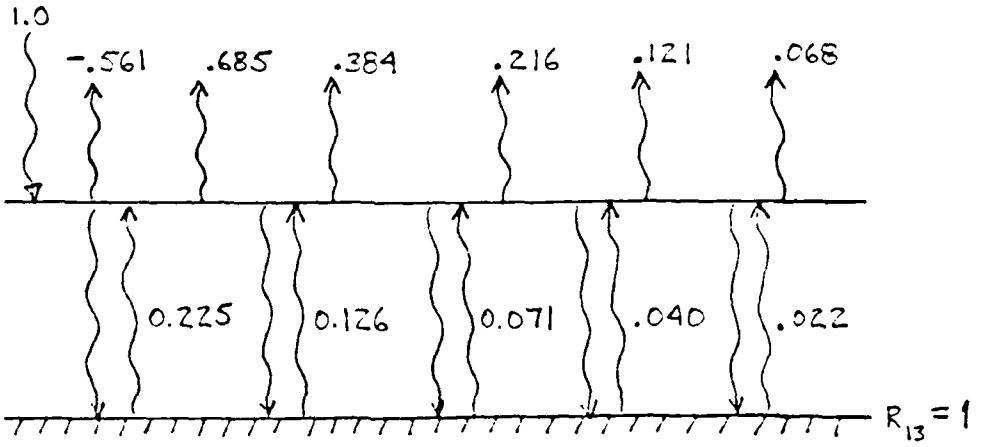

Figure A-5. Theoretical calculations for the expected reflected impulse response of the elastic layer

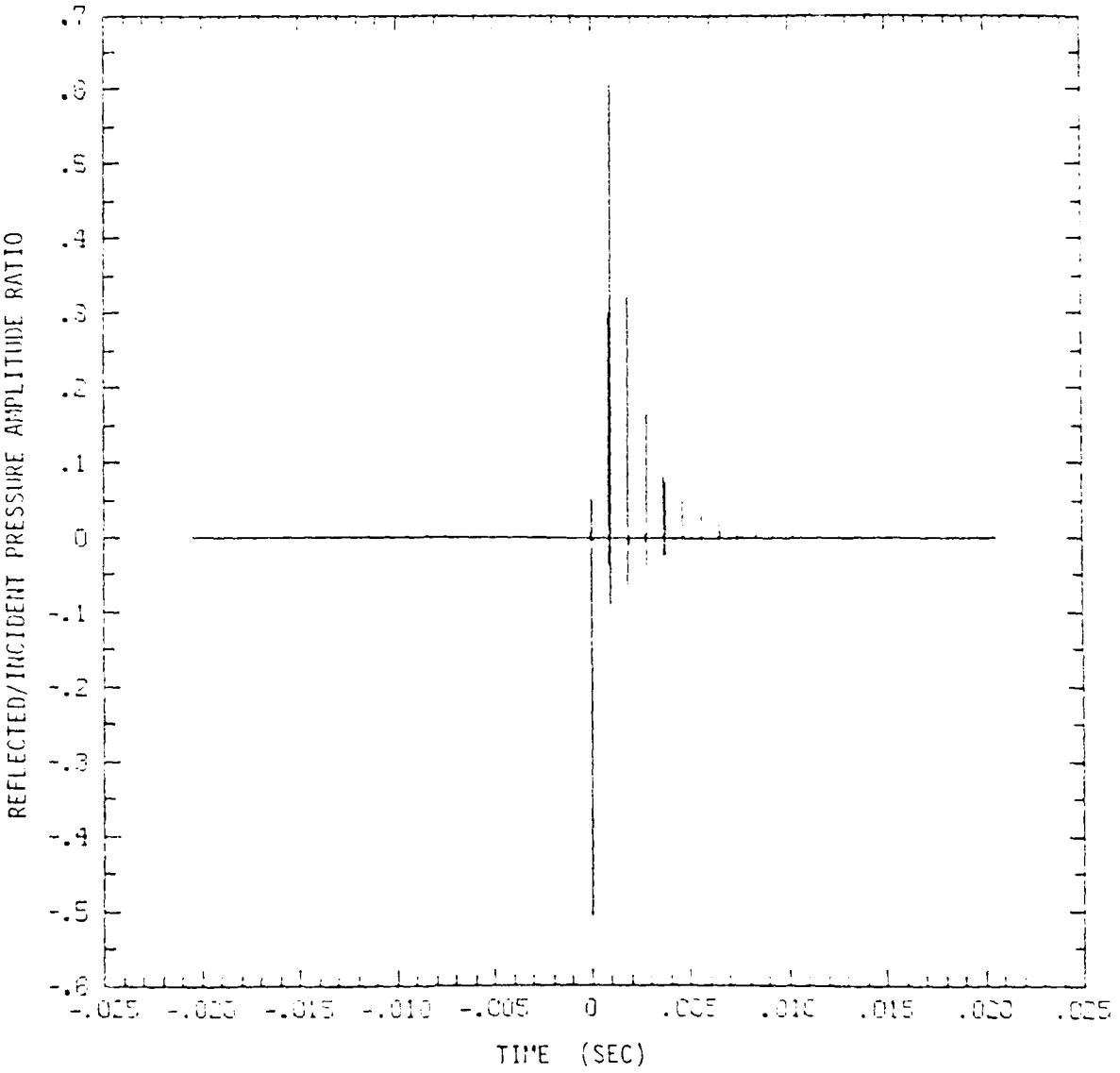

Figure A-6. Calculated reflected impulse response using a larger frequency range than for the results of Figure A-4.


DATE
ILME